PCCP

PAPER

View Article Online
View Journal | View Issue



Cite this: *Phys. Chem. Chem. Phys.*, 2019, **21**, 13268

# Determining the gas composition for the growth of BNNTs using a thermodynamic approach

Alexander Khrabry,*[a] Igor D. Kaganovich,[a] Shurik Yatom,[a] Vladislav Vekselman,[a] Jelena Radić-Perić,[b] John Rodman†[a] and Yevgeny Raitses[a]

Received 9th March 2019,
Accepted 28th May 2019

DOI: 10.1039/c9cp01342c

rsc.li/pccp

High-yield production of high-quality boron-nitride nanotubes (BNNTs) has been reported recently in several publications. A boron-rich material is evaporated using a laser or plasma in a nitrogen-rich atmosphere to supply precursor gaseous species for nucleation and growth of BNNTs. Either hydrogen was added or pressure was increased in the system to achieve high yield and high purity of the synthesized nanotubes. According to the widely-accepted "root grow" mechanism, upon gas cooling, boron droplets form first, then they adsorb nitrogen from the surrounding gas species, and BNNTs grow on their surfaces. However, what are the precursor species that provide nitrogen for the growth is still an open question. To answer this question, we performed thermodynamic calculations for determining the B–N mixture composition considering a broad set of gas species. For the first time, condensation of boron was taken into account and was shown to have a drastic effect on the gas chemical composition. $B_2N$ molecules were identified to be a major source of nitrogen for the growth of BNNTs. The presence of $B_2N$ molecules in a B–N gas mixture was verified by our spectroscopic measurements during laser ablation of boron-rich targets in nitrogen. It was shown that the increase of pressure has a quantitative effect on the mixture composition yielding an increase of the precursor density. Hydrogen addition might open an additional channel of nitrogen supply to support the growth of BNNTs. The nitrogen atoms react with abundant $H_2$ molecules to form $NH_2$ and then $NH_3$ precursor species, instead of just recombining back to inert $N_2$ molecules, as in the no-hydrogen case. In addition, thermodynamics was applied in conjunction with agglomeration theory to predict the size of the boron droplets upon growth of BNNTs. Analytical relations for the identification of crucial species densities were derived.



## I. Introduction

Boron-nitride nanotubes (BNNTs) attract significant interest because of their unique properties, such as high Young's modulus,[1,2] excellent thermal conductivity,[3] superhydrophobicity,[4] a relatively lower rigidity in the transverse direction[5] and chemical stability up to 900 °C in air. Single-walled BNNTs are wide band gap semiconductors with a very small dependence on chirality.[6] Carbon doping of BNNTs offers a possibility of tailored electrical properties of nanotubes.[7,8] BNNTs can potentially be applied for oncology therapies[9,10] and for water desalination.[11,12] There is an increasing number of studies devoted to the synthesis of BNNTs. A thorough review on BNNT production methods, properties and applications can be found in ref. 13.

Successful high-selectivity production of high-quality BNNTs has been reported in atmospheric and higher pressure systems, including arc ablation[14,15] and laser ablation[16–19] reactors and, more recently, in inductively-coupled plasma (ICP) systems.[20–22] The latter offers scalable high-yield production of BNNTs at relatively low cost. It is noteworthy that these methods enabled the production of BNNTs without the addition of any metallic catalysts in the synthesis process, unlike other methods.[23,24] In both these methods, solid boron or a boron-rich material in a bulk or powder form is evaporated in a nitrogen atmosphere using a laser or high-temperature ICP plasma forming a B–N atomic gas mixture at high gas temperatures. In colder regions, the gas condenses resulting in the formation of nanoparticles. A thorough review on BNNT synthesis methods can be found in ref. 25.

A commonly accepted mechanism for the formation of BNNTs from the condensing gas is the so-called "root-growth" mechanism, first proposed in ref. 16 based on the results of *ex situ* analysis, then supported in ref. 20 and 21, and later witnessed by *ab initio* molecular dynamic simulations and

[a] *Princeton Plasma Physics Laboratory, Princeton University, NJ, USA. E-mail: akhrabry@pppl.gov; Tel: +1 (609) 243-2550*
[b] *University of Belgrade, Serbia*
† Permanent address: University of Syracuse, NY, USA.

 

arc synthesis experiments.[26] According to the root-growth concept, when the B–N gas mixture cools down, boron gas condenses first and droplets of liquid boron form. Then, boron within the droplets reacts with nitrogen-containing radicals from the ambient gas, and BNNTs grow out from the droplet surfaces. However, what are the gas species that provide nitrogen for the BNNT growth is still an open question. In ref. 20, for instance, it is assumed that $N_2$ molecules might be precursors for the growth of BNNTs. However, it is questionable whether $N_2$ molecules can serve as precursors for the formation of periodic (hexagonal) B–N solid structures because this transformation is energetically unfavorable: $N_2$ molecules have a high binding energy of 9.8 eV whereas the B–N bond energy is about 4.0 eV. Other gaseous species such as atomic nitrogen N and BN, $BN_2$ and $B_2N$ molecules are more favorable precursors for the formation of hexagonal BN structures.

In recent molecular dynamics simulations,[27] several atomic and molecular gas species were tried as ''building blocks'' to produce solid BN structures. It was shown that tube-like and cage-like BN structures can be efficiently formed from BN molecules. However, these simulations have been performed with a pre-defined gas composition; in particular, pure BN gas and pure borazine gas were separately considered. In practice, the feedstock material is introduced into plasma, evaporates and is subsequently transported to the reaction zone.[20,21,28] In this zone, under definite temperature conditions, boron starts to condense and nanotubes are formed. In this process, the composition of the gas mixture cannot be arbitrary determined; it is determined by the chemical reactions between the gas species. What can be controlled is the feedstock material, the pressure and the temperature within the system and the buffer gas composition.[29–31] Molecular dynamics simulations are not capable of modeling long time-scale processes of material evaporation, cooling and condensation; different methods should be applied to determine the actual gas mixture composition at the nanoparticle growth.

Interestingly, for all plasma-based BNNT production methods (laser ablation, arc discharge and ICP plasma) rather low production rates were observed at atmospheric pressure: many of the boron droplets ended up with no nanotubes grown on them. The increase of the pressure up to 10 atm in ref. 20 and up to 20 atm in ref. 17 resulted in a substantially higher production yield of the nanotubes and their purity determined as a ratio of the nanotubes weight to the total synthesized product weight. There were also studies where even higher pressures were applied, up to 68 atm.[32] Another approach to increase the yield of BNNTs was found in ref. 21 and 22: it was shown that the addition of hydrogen to the working gas can increase the yield and purity of the nanotubes produced even without the increase of pressure. It is interesting to investigate the gas mixture compositions in these systems and to identify which gas species are crucial precursors for the efficient growth of BNNTs.

Thermodynamic modeling[33–35] is well suitable for determining the composition of a chemically reacting system close to the equilibrium state. There are several studies[36,37] devoted to determining the composition of the B–N gas mixture at various temperatures. In ref. 37, a broad set of gas species was considered including three atomic molecules $B_3$, $B_2N$ and $BN_2$. Intriguingly, $B_2N$ molecules were shown to be dominant species at lower temperatures corresponding to the formation of solid BN structures suggesting them as a main precursor for the growth of BNNTs. However, in previous thermodynamic computations,[36–38] condensation of boron was not taken into account (only gas phase species were considered) resulting in overestimation of boron-containing gas species densities at low temperatures where BNNTs grow.

In this paper, we present the results of thermodynamic calculations for the B–N system equilibrium composition at atmospheric and increased pressures with and without the addition of hydrogen. A broad set of B, N and H containing gas species from ref. 37 was considered with the thermodynamic data from ref. 39 and 40. Liquid boron and solid BN were taken into consideration as well. This allowed us to account for the condensation of boron and to determine the conditions for solid BN formation.

A similar thermodynamic approach was previously used in ref. 41–43 to calculate the carbon–helium gas mixture composition with condensation of carbon, and in ref. 44 and 45 to examine the gas mixture composition in a chemical vapor deposition process for the production of $MoS_2$ layers and in complex metal hydride systems for the storage of hydrogen. In ref. 42, the species density profiles in a carbon arc for the synthesis of nanoparticles were computed and compared to *in situ* measurements. A good agreement with the experimental data on the species density profile was obtained in ref. 42, despite the fast flow, sharp density gradients and oscillations of the arc showing that the chemistry is much faster than other processes and the equilibrium assumption can be applied when determining the mixture composition for synthesis applications. Computational results for the B–N system were verified by comparison with the optical emission spectroscopy (OES) data from our experiments on laser ablation of boron-rich targets in a nitrogen atmosphere and with OES measurements[22] in the ICP plasma reactor.

The paper is organized as follows. In Section II, a thermodynamic method based on minimization of Gibbs free energy for determining the equilibrium composition of a chemically reacting mixture containing gas, liquid and solid species is described. Section III is devoted to the results of the thermodynamic calculations and their analysis. In Section III.A, the effect of gas condensation on the gas mixture composition is studied. In Sections III.B and III.C, the effects of pressure variation and hydrogen addition on the mixture composition and density potential precursors for the growth of BNNTs are studied. Section III.D is devoted to the verification of the thermodynamics results *via* comparison to the spectroscopic data for the ICP reactor.[22] Section III.E describes the experimental setup used for the laser ablation of boron-rich targets and presents the OES measurement results. In Section III.F, the thermodynamics results are used in conjunction with a simple agglomeration theory to predict the size of the boron droplets

by the time when BNNTs start growing on them and they are solidified. In Section III.G, the analytic relations for the densities of the major mixture components are derived. Finally, the conclusions are provided.

## II. Methods for determining the equilibrium chemical composition

For mixtures containing few components, their composition can be conveniently determined using thermodynamic equilibrium constants for decomposition and ionization reactions, together with the mass conservation law and electrical neutrality, see ref. 46 and references therein. For more complex mixtures, as we have here, the number of chemical reactions between different species becomes very large, and a different approach, based on the minimization of the Gibbs free energy, is more suitable.

According to the second law of thermodynamics, when a thermodynamic system reaches the equilibrium state at given temperatures and pressures its Gibbs free energy is at its minimum. Constant pressure is a good approximation when considering any gas volume moving with the flow because the Mach numbers in the reactors are normally very low (much less than unity). Typically, the temperature variation characteristic time is larger than the time required for the chemical composition to change, and hence, the mixture composition can be considered to be in chemical equilibrium and the thermodynamic approach can be applied. The applicability of the thermodynamic approach to determining the chemical mixture composition in BNNT production reactors is discussed in detail in Appendix C. A simple description of the Gibbs free energy minimization method for gas mixtures can be found in ref. 34 and 35.

The Gibbs free energy of a multi-component system (or mixture) can be expressed as the sum of the chemical potentials of its individual component species $\mu_i$ multiplied by their quantities $N_i$ (numbers of atoms or molecules) within a closed system (arbitrary chosen volume moving with the fluid flow) under consideration as:[47,48]

$$G = \sum_i N_i \mu_i. \tag{1}$$

For the gas species, the chemical potential can be expressed (in ideal gas approximation) as:[35,47–49]

$$\mu_i = RT \ln \frac{p_i}{p_0} + G_i^{\mathrm{f}}(p_0, T) = RT\left(\ln x_i^* + \ln \frac{p}{p_0}\right) + G_i^{\mathrm{f}}(p_0, T). \tag{2}$$

Here, $G_i^{\mathrm{f}}(p_0,T)$ is the molar Gibbs energy of the component $i$ in its pure state, at standard pressure $p_0$ = 1 atm and given temperature $T$, or, in other words, it is the Gibbs energy of formation of species $i$ from its constituting elements in their standard states at temperature $T$ (the Gibbs energy of formation of any species in its standard state is commonly considered zero); $p_i$ is its partial pressure; $p$ is the pressure in the system, $x_i$ is the molar fraction of species $i$ among other gaseous species (excluding solid and liquid species):

$$x_i = \frac{N_i}{\sum\limits_{k \in \text{gas species}} N_k}. \tag{3}$$

For incompressible solid and liquid species, the energy does not depend on pressure, and the expression for the chemical potential reduces to:

$$\mu_i = G_i^{\mathrm{f}}(T). \tag{4}$$

The equilibrium composition of a mixture of known gaseous, liquid and solid components can be determined as a set of $N_i$ which gives the minimum value of the Gibbs energy (1) and satisfies constraints of conservation chemical elements of each sort of atoms within the system:

$$\sum_i a_{i,j} N_i = b_j N^*; \quad j = 1, 2, \ldots, m. \tag{5}$$

Here, $m$ is the number of different sorts of atoms (different chemical elements) within the system, $b_j$ is the mole fraction of element $j$ within the system, $a_{i,j}$ is the number of atoms of sort $j$ in species $i$, and $N^* = \sum\limits_{i \in \text{all}} \left( N_i \sum\limits_j a_{i,j} \right)$ is the total number of various atoms in all species within the system. Because the densities and molar fractions of species usually are of interest (not absolute numbers of atoms and molecules), $N^*$ can be chosen arbitrary.

The charge conservation needs to be maintained as well:

$$\sum_i Z_i N_i = 0. \tag{6}$$

Here $Z_i$ is the charge number of species $i$; $Z_i = -1$ for electrons.

The substitution of $\mu_i$ defined by (2) and (4) into (1), using (3), yields the following function of species quantities $N_i$ to be minimized:

$$RT \sum_{i \in \text{gas}} N_i \left( \ln N_i - \ln \left( \sum_{k \in \text{gas}} N_k \right) + \ln \frac{p}{p_0} \right) + \sum_{i \in \text{all}} N_i G_i^{\mathrm{f}}(p_0, T) \to \min. \tag{7}$$

Here, $N_i$ are the absolute quantities of species within the system. The densities and partial pressures of gaseous species $n_i$ can be derived from their molar fractions, $x_i^*$, defined in (3):

$$p_i = x_i p; \quad n_i = x_i \frac{p}{kT}. \tag{8}$$

The simultaneous consideration of solid and liquid species allows accurate accounting for condensation/solidification occurring in the considered gas volume at a constant pressure and a slowly changing temperature.

For B–N and B–N–H mixtures we consider a broad set of species including various triatomic molecular gases from ref. 37. The Gibbs energies of formation $G_i^{\mathrm{f}}(p_0,T)$ for gases N, $N_2$, $N_3$, B, $B^+$, $B_2$, H, $H_2$, NH, $NH_2$, $N_2H_2$, $N_2H_4$, $NH_3$, BH, $BH_2$, $BH_3$, and $G_i^{\mathrm{f}}(T)$ for liquid/solid B and solid (crystalline) BN were taken from NIST-JANAF ref. 39 where they are tabulated as functions of temperature at atmospheric pressure. For the sake

 

of simplicity, only atomic boron ions were considered; ions of other species have very low densities in these equilibrium calculations with the temperature range of interest (below 6000 K).[36,37]

Unfortunately, for other gas species observed in plasma and laser ablation of boron-rich targets in an inert gas atmosphere, such as $B_2N$,[50–52] $B_3$,[50,53] and $BN_2$ molecules, the thermodynamic data are not provided in tables.[39] Nevertheless, for these molecules, the free energy of association from the constituting atoms (in some other sources also referred as dissociation energy) was computed *ab initio* in ref. 40 using the quantum chemistry package Gaussian-86.[54] These data allow us to easily obtain the Gibbs energy of formation for these molecules which can be self-consistently used with other Gibbs free energy data on species from ref. 39:

$$G_i^{\mathrm{f}}(p_0, T) = \sum_j a_{i,j} G_j^{\mathrm{f}}(p_0, T) - \Delta G_i^{\mathrm{f}}(T). \qquad (9)$$

Here, $G_i^{\mathrm{f}}(p_0,T)$ is the Gibbs energy of formation of a molecule $i$, $\Delta G_i^{\mathrm{f}}(T)$ is its free energy of association,[40] the summation in the right-hand side is performed over various atoms within the molecule, $G_j^{\mathrm{f}}(p_0,T)$ is the Gibbs energy of the atoms in the gaseous state,[39] and again $a_{i,j}$ is the number of atoms of sort $j$ in a molecule $i$. Note that in ref. 40, for molecules having several isomers, *e.g.*, $B_2N$, the individual contributions of various isomers were weighted and the global thermodynamic quantity was presented making the implementation of the data very convenient.

In principle, even larger molecules consisting of B and N atoms, such as $B_2N_2$, $BN_3$ and $B_3N$, were observed in some of the experiments.[51,52] However, the lack of thermodynamic data for these molecules did not allow us to take them into consideration. In this regard $B_2N$ can be viewed as a proxy for other larger molecules, similar to what was observed for carbon where many molecular species can be accounted for.[41,55]

Additional complication is that the thermodynamic data for BN molecules[39] are provided with a very high level of uncertainty. The free energy of formation is calculated based on the dissociation energy for which uncertainty is about 70%: its value varies between 4 eV and 7 eV under standard conditions, depending on the literature. Such an ambiguity in the energy of formation would result in substantial uncertainty (of several orders of magnitude) in the computed BN molecule density in the equilibrium B–N mixture. It is noteworthy that in ref. 39 rather old literature was considered when constructing the table for BN molecules, 1964 and before. Newer sources[40,56–60] are more consistent on BN dissociation energy values under standard conditions, providing values varying from 3.9 eV to 4.5 eV. A possible explanation for such a variety of the dissociation energy values in old papers can be deduced from ref. 59 where it is explained that the binding (or dissociation) energy of the BN molecule depends on whether it is considered to be in the ground state $^3\Pi$ or the excited state $^1\Sigma$. For the ground state, adequate for our temperatures of interest, the binding energy is about 4 eV. For our thermodynamic modeling, we calculated the free energy of association $\Delta G_i^{\mathrm{f}}(T)$ for BN molecules using the thermodynamic data from ref. 40, which is found to be consistent with the data for other molecules. We also tried the thermodynamic data for BN from a newer source,[58] and there were some quantitative changes in the BN densities but the picture did not change qualitatively. The energy was calculated from the equilibrium constant $K_{\mathrm{f}}$ for the formation reaction: $\Delta G_i^{\mathrm{f}}(T) = -RT \ln K_{\mathrm{f}}$.

# III. Results and discussion

## III.A. Effect of boron condensation on the species densities

The computed composition of the B–N mixture (with no hydrogen) is shown in Fig. 1 and 2 as a function of temperature. Fig. 1 shows the effect of boron condensation on species densities. Two computational runs were performed. In one run, single phase calculations were performed – only gas phase species were considered. Their densities are presented partially as solid lines for $T > 4137$ K (4137 K is the boiling point of liquid boron at atmospheric pressure) and dashed lines, for $T < 4137$ K. The different colors represent different species. In another run, liquid boron and solid BN were added to the system allowing accounting for boron condensation and solid BN formation. The results of this run are plotted with solid lines. In both computational runs, the mole fractions of boron and nitrogen elements within the mixture were the same, 45% and 55% respectively; pressure is atmospheric. This boron fraction was chosen arbitrary here; the effect of boron fraction is discussed in more detail in the following section. Though a full set of boron- and nitrogen-containing species was modeled, only densities of boron-containing species were affected by the condensation. For the sake of keeping the plots in Fig. 1 legible, only these species are shown; other species are shown in the following subsections. $BN_2$ molecules have very low densities compared to other species and are not plotted in Fig. 1.

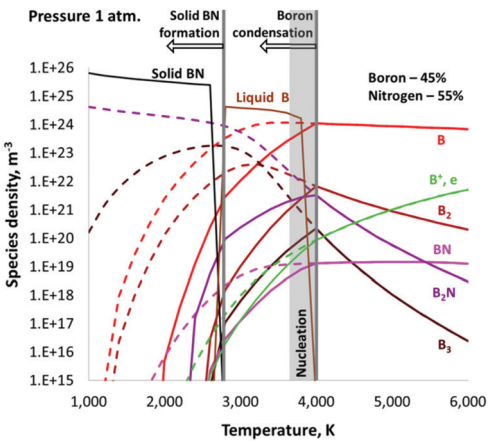


Fig. 1 Effect of boron condensation on gas species densities in the B–N mixture. Solid lines – results obtained with accounting for the condensation; dashed lines – condensation not accounted for. Though a full set of species was modeled, only densities of boron-containing species are affected by the condensation and plotted here. Condensation of boron has a drastic effect on the densities of all boron-containing gas species reducing their densities by orders of magnitude. This effect is very important when determining gas species surrounding boron droplets at temperatures of solid BN formation.

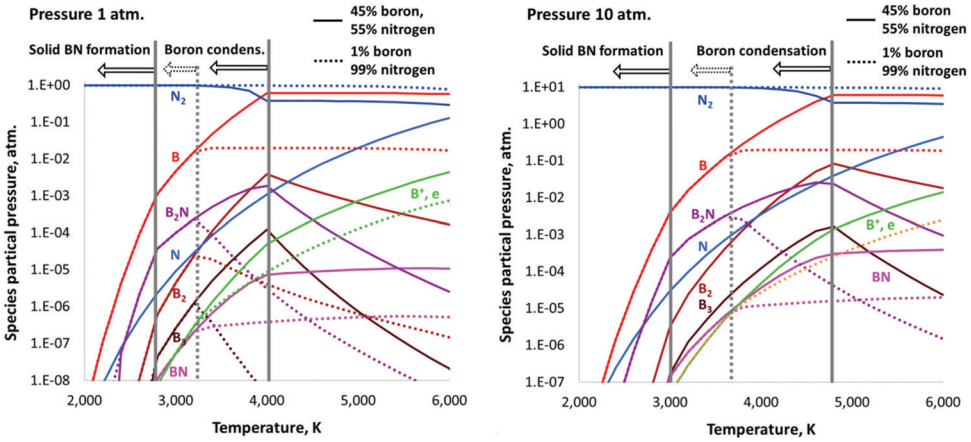


Fig. 2 Composition of B–N mixtures at pressures 1 atm (left) and 10 atm (right) having boron to nitrogen ratios 45 to 55 (solid lines) and 1 to 99 (dotted lines). Boron condensation is taken into account; the partial pressures of gas phase species are plotted as functions of temperature. The temperatures of boron condensation and solid BN formation are shown by vertical grey lines. The fraction of boron within the mixture affects the composition of the gas species only at higher temperatures, before boron condensation starts. When the condensation takes place, the gas species composition is determined merely by the boron vapor saturation curve. At the temperature of solid BN formation, $B_2N$ has the highest density among nitrogen containing species, after $N_2$, and can be suggested as the major source of nitrogen for the formation and growth of BNNTs. With the increase of pressure $p$, the densities of N, BN and $B_2N$ increased as $\sqrt{p}$ (as explained in Section III.G), while the ratios between the species densities remained practically the same.

From this figure it is clear that boron condensation has a drastic effect on densities of all gas phase boron-containing species. When the gas mixture cools down and the temperature reaches 4000 K, thermodynamics predicts that boron starts to condense, see line "Liquid B", which shows the density of boron atoms within liquid droplets in a unit gas volume. The condensation at definite temperature can occur when the system becomes "oversaturated" with respect to the partial pressure of boron atoms. As a consequence of the formation of liquid boron, the amount of boron in the gas phase is lowered and the equilibrium density ratios among boron-containing species B, BN, $B_2N$, *etc.* in different gas phase reactions are disturbed. To reestablish this equilibrium, according to Le Chatelier's principle, the chemical reactions are shifted in direction of the formation of B atoms by additional dissociation of the boron-containing molecules, leading to further formation of liquid boron until the heterogeneous equilibrium between gas phase boron and liquid boron is completed. This also means that the partial pressure of boron atoms is equal to its saturation level value, $p_B^s$ (which is a function of temperature, only); and the solid line curve for B at $T < 4000$ K denotes the boron saturation vapor pressure curve. That value and thermodynamic equilibrium constants of chemical reactions determine the partial pressure values of other boron containing compounds BN, $B_2N$, $B_2$ *etc.* This question will be addressed in more detail in Section III.G, where analytical relations for the species densities as functions of temperature are derived.

When the temperature decreases to 3800 K, most of the boron has already condensed. When the temperature approaches about 3000 K, thermodynamics predicts that the formation of solid BN should begin, see line "Solid BN". Because initially there was slightly more nitrogen than boron in the mixture, see also Fig. 2, we can conclude that almost all liquid boron is consumed to form solid BN and some nitrogen is left in the form of $N_2$ gas to maintain pressure within the system. Here and in the subsequent figures, the temperatures corresponding to initiation of boron condensation and formation of solid BN are marked in the figures with vertical grey lines.

Formation of solid BN involves, besides boron liquid, also nitrogen and boron containing gas phase species BN, $B_2N$ *etc.* Their densities are determined by heterogeneous equilibrium and are considerably lower compared to those computed using a one-phase procedure which does not take condensation of boron into account (denoted by dashed lines at $T < 4000$ K in Fig. 1).

Note that Gibbs free energies[39] for liquid boron and solid BN, which were used in present thermodynamic calculations, were obtained without accounting for the surface energy effects for nanoparticles. They are valid for such relatively large volumes of liquid/solid that the surface effects can be neglected. However, at the initial stage of condensation, when droplets of liquid boron nucleate and are very small (on a sub-nanometer scale), the surface effect leads to a barrier for the nucleation of droplets.[61–63] In other words, while a gas mixture is cooling down, condensation does not immediately start when the temperature reaches the saturation point predicted by the thermodynamics. The calculations[64–66] for aluminum and our calculations using a Nodal General Differential Equation (NGDE) solver[65] and theoretical findings[67] for nucleation of the boron droplets have shown that no condensation occurs until the actual gas pressure exceeds the saturated vapor pressure predicted by the thermodynamics about five times (*i.e.*, the super saturation degree is about 5 instead of one) with a very weak dependence on the gas cooling rate. This super-saturation degree corresponds to a temperature of about 300 K below the saturation point for boron at atmospheric pressure

 

(due to the very strong dependence of vapor pressure on gas temperature). After this, nucleation and growth of boron droplets occur very rapidly, the surface energy effects for the droplets become negligible, the boron vapor condenses onto the droplets, an equilibrium between gas and liquid phases is reached, and the present thermodynamic predictions of the mixture compositions become valid.

In other words, the actual condensation temperature is about 300 K lower compared to the one predicted by thermodynamic calculations. In the grey shaded region denoted ''Nucleation'' in Fig. 1, the mixture is well described by the solution with no condensation (dashed lines). At the left boundary of the shaded area the mixture composition changes abruptly switching to the solution with condensation (solid lines).

Note that the main focus of this paper is to determine the gas composition at temperatures corresponding to the formation of solid BN structures (*e.g.*, nanotubes), and these temperatures (2000–2400 K; see ref. 26) are substantially lower than the temperature of boron condensation ($\approx$4000 K; see Fig. 1). The processes involved in the nucleation of boron droplets are out of the scope of this paper. Therefore, for the sake of simplicity of the subsequent figures, only the thermodynamic results of the calculations considering liquid boron (solid lines in current notations) corresponding to gas in equilibrium with liquid are plotted. The assessments presented in Appendix C show that thermodynamic predictions for densities of major mixture components at the temperature of solid BN formation are applicable to BNNT production reactors.

### III.B. Effect of pressure increase on the B–N mixture composition

In Fig. 2, the composition of the B–N mixture is shown for pressures 1 atm and 10 atm. The partial pressures of the gas phase species are plotted as functions of temperature. $N_3$ molecules have low densities compared to other species and are not plotted. The temperatures of boron condensation and solid BN formation are shown by grey vertical lines. In order to show the effect of the boron fraction on the mixture composition, in addition to previously considered boron to a nitrogen ratio of 45 to 55, the results for a mixture with only 1% of boron are plotted.

Apparently, reduction of the boron fraction affects the boron partial pressure at higher temperatures, when no condensation takes place and all species are in the gas phase. As seen from the plots, it results in reduction of temperature at which boron vapor becomes saturated and condensation starts. At temperatures lower than this, the fraction of boron in the gas phase and the chemical composition of the gas phase are generally determined only by the saturation vapor pressure and do not depend on the initial fraction of boron within the mixture. This result is also confirmed by analytical derivations presented in Section III.G. An amount of boron in the liquid phase is obviously affected by its initial fraction; the initial amount of boron also affects the size of boron droplets formed during the condensation, as discussed in Section III.F.

When boron starts condensing, molecular nitrogen, $N_2$, becomes the major component in the mixture, with several orders of magnitude higher density than other components. $N_2$ molecules have a high dissociation energy of 9.8 eV and can hardly be dissociated at boron droplets (unless they penetrate deep into boron[26]); hence, they are unlikely to be effective precursors for the formation of B–N nanostructures. Among other nitrogen containing species, $B_2N$ has the highest density, an order of magnitude higher than its closest competitor, atomic N. This is due to its bond energy of about 6 eV.[40] $B_2N$ molecules can be disassembled at surfaces of boron droplets[26] and can be suggested as major precursors for the growth of BNNTs. Atomic nitrogen may contribute to the growth of BN nanostructures as well.

The increase of pressure from 1 atm to 10 atm resulted in a $B_2N$ partial pressure increase by a factor of 10 at temperature of solid BN appearance, possibly explaining the increase of nanotube production yield observed in ref. 17 and 20.

### III.C. Effect of hydrogen addition

As proposed in ref. 21, hydrogen addition could support the BNNT growth *via* the formation of N–H containing gas phase species that could serve as nitrogen sources to boron droplets on which the BNNTs grow (see Fig. 5 in ref. 21). In this section, the gas phase mixture composition is analyzed to identify these species. The mixtures with 5% and 30% hydrogen addition at atmospheric pressure are considered. The results of the chemical composition computations are shown in Fig. 3 and 4. Fig. 3 shows the plots for densities of nitrogen-containing gas species. The rest gas species are shown in Fig. 4. Note that $N_2H_2$ and $N_2H_4$ molecules were considered in the simulations but are not plotted because of their negligibly low densities.

As seen from Fig. 3, even with substantial addition of hydrogen (30%), $B_2N$ is still the major nitrogen-containing gas phase component (after $N_2$) at the temperature of the appearance of solid BN (2800 K). Nevertheless, with further decrease of temperature, the densities of all boron-containing species (including $B_2N$) continue to drop rapidly, whereas the density of ammonia $NH_3$ molecules grows. Soon, at a temperature of about 2600 K, $NH_3$ becomes the major nitrogen-containing species, after $N_2$. NH and $NH_2$ molecules are also present but have much lower densities than $NH_3$ under these conditions and cannot noticeably affect the growth of BNNTs. As discussed in Appendix C, the rates of NH and $NH_2$ destruction and consumption are sufficiently high to reduce their density in accordance with the thermodynamic prediction at the temperature of BNNT growth.

As shown in ref. 68 and 69, molecules of ammonia dissociate at surfaces of boron droplets releasing hydrogen into a gas phase and can serve effectively as feedstock of nitrogen for the growth of solid BN structures. $NH_3$ is known to serve effectively as a nitrogen source for BNNTs in low temperature (1500 K) furnace reactors.[70,71] It is plausible that $NH_3$ molecules provide nitrogen for further growth of BNNTs at lower temperatures, when the amount of $B_2N$ molecules is significantly lowered due to the condensation of boron, and boron droplets are not yet

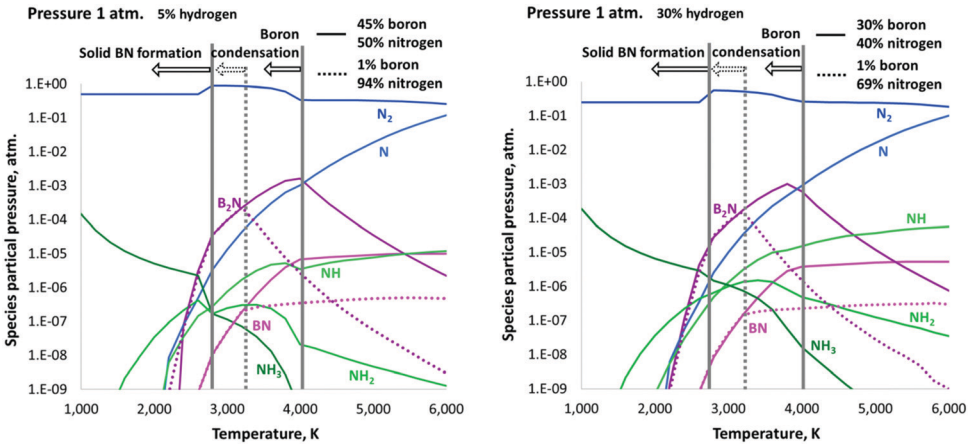


Fig. 3 Composition of B–N–H atmospheric pressure mixtures with hydrogen fractions of 5% (left) and 30% (right). Only nitrogen-containing species are plotted here (for other species, see Fig. 4). The temperatures of boron condensation and solid BN formation are represented by vertical lines. With high hydrogen fraction, the $NH_3$ molecules become prominent near the temperature of solid BN appearance, and may serve as a nitrogen source for the growth of BNNTs.

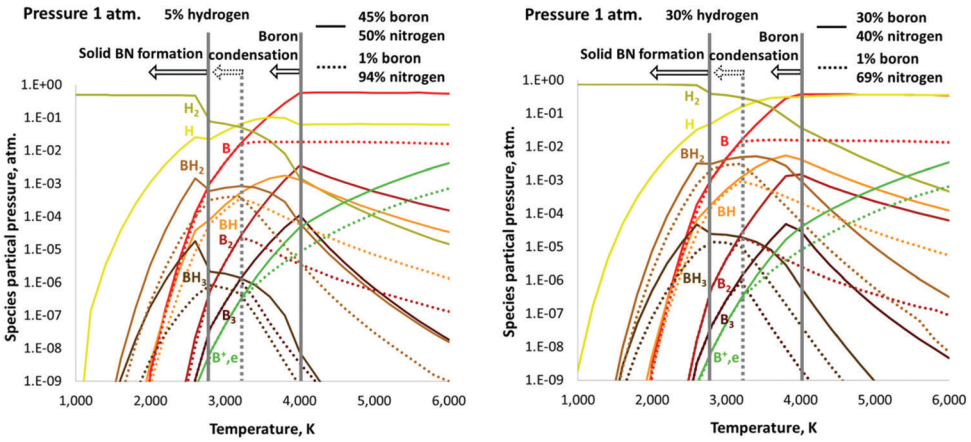


Fig. 4 Composition of the B–N–H atmospheric pressure mixtures with hydrogen fractions of 5% (left) and 30% (right). Only species that do not contain nitrogen are plotted (for nitrogen-containing species, see Fig. 3). The temperatures of boron condensation and solid BN formation are represented by vertical lines.

solidified, which occurs at a temperature of about 2350 K. In other words, the addition of hydrogen might open an additional channel of nitrogen supply for growing BNNTs *via* formation of $NH_3$ molecules. This might explain a higher yield production of longer nanotubes observed in the case of hydrogen addition.[22]

Even though it is energetically favorable, as predicted by the thermodynamics, a common concern regarding ammonia formation from $H_2$ and $N_2$ is that the process is known to be very slow at low temperatures due to the high activation energy barrier associated with the need to dissociate molecular nitrogen.[72] In a well-known Haber–Bosch process[72] invented in the beginning of the 20th century, a metallic (iron) catalyst and a high pressure of about 200 atm are required in order to speed up the $N_2$ dissociation reaction and to produce high yield of $NH_3$; in experiments[73] ammonia is produced during $H_2$ desorption in metal hydride systems. But in high-yield BNNT synthesis systems, there are no metallic catalysts; $N_2$ molecules do not dissociate on the liquid boron surface.[26] Can $NH_3$ be produced there at a sufficient rate? Note that the Haber–Bosh process and experiments[73] were run at a constant temperature of 800 K, whereas in nanosynthesis reactors, the BNNTs grow at temperatures above 2300 K, and the mixture components originate from higher temperature regions with a sufficient amount of atomic nitrogen. As discussed in Appendix C, the nitrogen atoms react quickly with abundant $H_2$ molecules forming sufficient amounts of $NH_2$ and then $NH_3$ molecules in accordance with the thermodynamic prediction. $NH_2$ molecules serve as reaction intermediates; they transform to $NH_3$ at a high rate resulting in a considerably higher density of the latter.

### III.D. Comparison to the OES data from ref. 22

In ref. 22, high yield production of high quality BNNTs was achieved in an ICP plasma reactor at atmospheric pressure with addition of up to 24% hydrogen to the gas mixture.

 

Computational Fluid Dynamics (CFD) Simulations of gas flow with heat transfer were performed. The temperature and velocity profiles were obtained. Evaporation of BN powder and transport of BN vapor were simulated. Complete evaporation of the BN feedstock is suggested. However, chemical reactions within the system were not considered, BN gas was modeled as a non-reacting admixture, and the gas mixture composition was not predicted in the modeling. Instead, the optical emission spectra were measured at several locations within the reactor.

Simulation results[22] on the BN density and the temperature allow us to estimate the molar fraction of boron within the gas. The data[22] on the boron fraction and the gas temperature can be used as an input for the thermodynamic modeling to compute the gas mixture compositions at given locations within the reactor. The applicability of the equilibrium thermodynamic description to the processes in the BNNT synthesis reactor is discussed in Appendix C. These results can be compared to the OES data from ref. 22. Note that passive spectroscopy was utilized in ref. 22 which does not provide quantitative data on species densities. The emission of polyatomic molecules is weak, and their spectral lines were not detected at any location within the reactor. Thereby, these experimental data only allow qualitative comparison between the densities of atomic/diatomic species predicted by the modeling and their visibility in the emission spectra at various locations within the reactor. The results of this comparison are listed in Table 1. A similar qualitative comparison between the calculations and the experimental results was performed, for instance, in ref. 45.

The first location where the spectrum was measured (0.38 m away from the inlet) had a gas temperature of about 5000 K. The BN gas molar fraction is about 2% meaning about 1% of the boron molar fraction. The NH molecular emission lines are prominent, and N atomic spectral lines and $N_2$ molecular bands were observed as well. Atomic B emission lines were detected as well as emission bands from BH and NH radicals. The spectral lines of atomic H were clearly identified, while the relative weakness of the $H_2$ molecular band suggests effective dissociation of $H_2$ into H atoms. A trace of BN molecules was observed but its intensity was much weaker than those of BH or NH radicals. These observations agree with the results of our thermodynamic modeling (see Fig. 4). The NH molecules have considerable density (molar fraction $10^{-4}$ in the case of high fraction of hydrogen within the mixture system). Atomic boron has high density (molar fraction 0.02; almost all boron is in the atomic form). Hydrogen is mostly present in the atomic form; the density of the $H_2$ molecules is about 3.5 orders of magnitude lower. The density of the BN molecules is two orders of magnitude smaller than those of both BH and NH molecules.

At the next downstream locations where OES measurements were performed (0.48 m and 0.88 m from the inlet) corresponding to temperatures of 3700 K and 2400 K respectively, spectral lines of B atoms and NH molecules were no longer observed, whereas BH molecules and H atoms were still detected. The BH molecular band at 0.48 m (3700 K) is the most prominent one. These observations agree well with the thermodynamic results (Fig. 4): at a temperature of about 2400 K, the density of H radicals is still high; it is of about the same order of magnitude as it was at 5000 K. However, the density of the boron atom reduces about two orders of magnitude at 2400 K due to condensation of boron. The density of BH molecules at 3700 K is higher than that at 5000 K, and at 2400 K is about the same as at 5000 K.

Note that in ref. 22, the enhanced growth of BNNTs in the case of hydrogen addition to the gas mixture was attributed to the presence of NH radicals in the mixture. It was assumed that BNNTs start to grow immediately when boron starts to condense, at temperatures slightly below 4000 K, where the density of NH radicals is high. However, the results of thermodynamic modeling suggest that nanotubes and other solid BN structures start growing at temperatures below 2800 K where the density of NH molecules is rather low, which is in agreement with the OES measurements. $NH_3$ molecules have a higher density under these conditions, as discussed in the previous section.

### III.E. Laser ablation of boron-rich targets: experimental setup and results

The sketch of the setup and the imaging using an iCCD is shown in Fig. 5. The wavelength calibration was conducted using Hg and Xe calibration lamps: the resulting diffusion relation was determined to be 0.18–0.16 A per pixel and the instrumental width for a slit width of 50 micron is $\sim$1 A. The experiments of laser ablation of the BN target were conducted

Table 1 Qualitative comparison between the results of the OES measurements[22] and the thermodynamic modeling. Good qualitative agreement is observed between the species densities predicted by the modeling and their visibility by the OES measurements

| Location of the spectra measurement; gas temperature | Species detected in the OES spectra[22] | Species predicted by the thermodynamic modeling and their molar fractions |
|---|---|---|
| Distance from the inlet: 0.38 m | Detected: N, $N_2$, NH, B, BH, H | N ($2 \times 10^{-2}$), $N_2$ ($2 \times 10^{-1}$), NH ($3 \times 10^{-5}$), B ($2 \times 10^{-2}$), BH ($3 \times 10^{-5}$), H ($3 \times 10^{-1}$) |
| Temperature: 5000 K | Weak signal: BN, $H_2$ | BN ($3 \times 10^{-7}$), $H_2$ ($3 \times 10^{-3}$) |
| Distance from the inlet: 0.48 m | Detected: BH, H | BH ($3 \times 10^{-4}$), H ($3 \times 10^{-1}$) |
| Temperature: 3700 K | Not detected: B, NH | B ($2 \times 10^{-2}$), NH ($10^{-5}$) |
| Distance from the inlet: 0.88 m | Detected: H | H ($10^{-2}$) |
| Temperature: 2400 K | Weak signal: BH | BH ($3 \times 10^{-6}$) |
| | Not detected: B, NH | B ($3 \times 10^{-6}$), NH ($3 \times 10^{-8}$) |

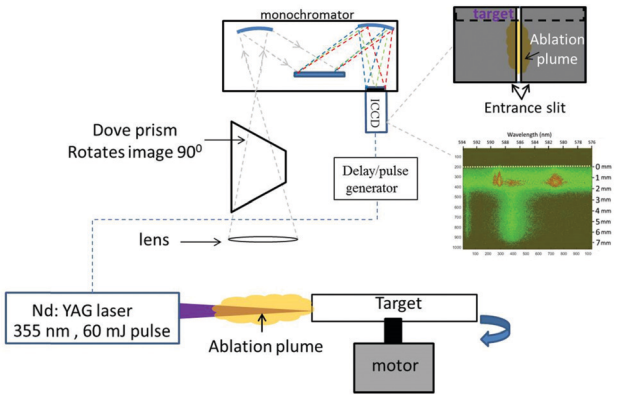


Fig. 5 Experimental setup in the laser ablation experiment of the BN target.

in a chamber in order to control the gas environment. Prior to the experiment the chamber was evacuated and subsequently filled with either He or $N_2$ gas, up to a pressure of $P$ = 400 Torr. The details of the experimental setup are provided in Appendix A.

The identification of atomic species was done according to the NIST database[74] and the molecular species – according to ref. 75 and 76. Overall we have detected 3 band-heads of $B_2N$ at 488.1, 504.3 and 519.5 nm,[76] in experiments of BN target ablation in He and in $N_2$ environments. Fig. 6 shows the temporal evolution of the spectrum in the range of 480–497 nm within the first microsecond after the laser pulse, in the experiment conducted in He-filled chamber. The presented spectra were captured with exposure of 50 ns, in 50 ns intervals, accumulating the emission from 100 shots. In order to show the temporal evolution in a single figure the intensity of each spectrum was normalized in the range (0, 1). The boron and nitrogen ion lines are prevalent in the spectrum, following the laser impact on the BN target. These lines are strongly broadened, owing to the high density and temperature in the spatial-temporal vicinity of the laser impact. After ~300 ns they disappear and the $B_2N$ band emerges. Molecular $B_2N$ emission bands were observed for tens of microseconds, after the laser shot. A more detailed analysis of these results will be described in a separate paper. For the purpose of this work, the most important result is the observation of molecular species in the ablation plume which were also predicted by thermodynamic calculations.

To summarize, spectroscopic measurements verify the presence of $B_2N$ molecules in the B–N gas mixture at nearly atmospheric pressure. Interestingly, immediately following the laser pulse the $B_2N$ molecules are not detected, only the precursors (B and N ions and atoms) are detected; it takes several fractions of microseconds for $B_2N$ molecules to appear. This behavior supports the point that $B_2N$ molecules do not come directly from the target; they are formed by chemical reactions in the gas phase, as suggested by the thermodynamic modeling.

### III.F. Estimation of boron droplets size upon formation of BNNTs in an ICP and arc discharge reactors

Experiments[21,77] have shown that the diameters of BNNTs are strongly correlated with the sizes of catalyst droplets on which they grow, and the formation of nano-sized boron droplets with suppression of their growth is important for the production of small-diameter BNNTs. A similar effect is well known for carbon nanotubes (CNTs).[78] Unfortunately, not much research was done for BNNTs as it was done for CNTs. Besides, some sources[15,16] do not report correlation between the droplet and nanotube diameters. Thorough experimental and theoretical research is required to answer a question if there is a correlation and how to control the properties of the nanotubes produced. This research is out of the scope of this paper. In this section, we provide a simple expression for boron droplets size, which can facilitate this research.

Growth of boron droplets can be divided into two stages:[61] (1) the nucleation stage refers to a statistical process of boron atom aggregation into clusters in which stable boron droplets are formed; (2) the agglomeration stage refers to a process of droplet growth *via* collisions with each other leading to their coagulation into larger droplets.

In a cooling gas mixture, nucleation of droplets does not occur immediately when the conditions for the gas condensation are met as predicted by thermodynamics. This is due to the energy barrier for the formation of stable droplets.[61] For boron, the "delay" is about 300 K, with a very weak dependence on the gas cooling rate. When this condition on the temperature is met, nucleation occurs abruptly, and many stable droplets are rapidly formed. Once the droplets are formed, their growth is governed by coagulation (droplets merge upon colliding with each other).

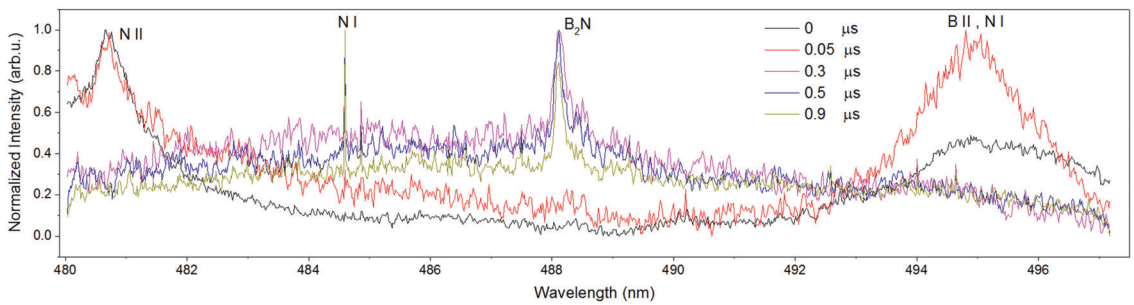


Fig. 6 Temporal evolution of the spatially-integrated, ablation spectrum of solid BN in He ($P$ = 400 Torr), in the 480–497 nm range. The intensities were normalized in 0–1 range in order to show the spectra on the single plot.

 

If the gas is ionized, the particles may become charged, which in turn can affect the coagulation process, as is shown *e.g.*, in ref. 79 and 80. However, in ref. 79 and 80 and other, low pressure plasma was typically considered, where the electron temperature reaches 5 eV (typically maintained by an RF source) while the gas and the particles are at a room temperature. Such an electron temperature provides a high ionization rate sufficient to compensate the loss of charge particles due to the ion (positive ion-electron) recombination at the droplet surfaces, and maintain the plasma. In atmospheric (and higher) pressure reactors considered in this paper, the electron temperature is close to the gas temperature (is about 0.3 eV in the coagulation region). At this temperature, the ionization rate is quite low and plasma will be virtually immediately extinguished *via* interaction with the droplets as soon as they appear, as is shown in detail in Appendix B.

Thereby, coagulation will occur in a neutral gas with neutral particles, and a simple agglomeration theory[81] can be employed to describe this process. This theory was applied in ref. 43 to describe the growth of carbon nanoparticles, and good agreement on the size of particles with results of *in situ* measurements[82] was obtained. The initial size of the nucleated particles is very small (containing tens of atoms[66]) compared to grown particles and can be neglected. With this simplification, a relation for the average diameters of the nanoparticles is:[43]

$$D = (2r_0)^{9/5} n_0^{2/5} \left(\frac{4\pi k T}{m_B}\right)^{1/5} t^{2/5}. \quad (10)$$

Here, $t$ is the time elapsed from the beginning of particle agglomeration, $r_0 \approx 1.2 \times 10^{-10}$ m is the Wigner–Seitz radius for boron describing the distance between the atoms in a boron droplet, $n_0$ is the density of the boron atoms in the gas at the beginning of condensation, $k$ is the Boltzmann constant, $m_B$ is the mass of the boron atom and $T$ is the temperature.

Constant temperature is assumed in (10), which is not exactly the case for a cooling gas; however, typically temperature variation between nucleation of boron droplets and formation of BNNTs is rather small (about 20–30%), and the temperature is raised to a small power in (10). Hence, temperature variation can be neglected for simplicity, and average temperature $T = 0.5(T_{nucl} + T_{end})$ can be used in (10) resulting in a very small error. Here, $T_{nucl}$ is the predicted temperature at which nucleation of boron droplets takes place and agglomeration initiates, which can be predicted by thermodynamics for a gas mixture with a given molar fraction of boron (300 K should be subtracted to account for the nucleation energy barrier). $T_{end}$ is the final temperature at which the size of the nanoparticles should be determined. With a constant cooling rate $\dot{T}_0$, (10) can be transformed:

$$D = (2r_0)^{9/5} n_0^{2/5} \left(\frac{2\pi k (T_{nucl} + T_{end})}{m_B}\right)^{1/5} \left(\frac{T_{nucl} - T_{end}}{\dot{T}_0}\right)^{2/5} \quad (11)$$

$T_{end}$ can be taken equal to the temperature at which the formation of BNNTs and other solid BN structures takes place, $T_{BNNT}$, if the size of the boron droplet upon formation of BNNTs is of interest. Alternatively, $T_{end}$ can be taken equal to the temperature of boron solidification, $T_{B\_solid}$, if the final size of the boron droplets is of interest.

In the ICP reactor,[22] pressure is 1 atm and the molar fraction of boron is about 1% yielding a nucleation temperature of 3500 K and a solid BN formation temperature $T_{BNNT}$ = 2800 K, according to the thermodynamic computations (see Fig. 2 and 4). The temperature of boron solidification is $T_{B\_solid}$ = 2300 K.[39] Due to the energy barrier for the nucleation, the actual nucleation temperature is 300 K lower than that predicted by the thermodynamics: $T_{nucl}$ = 3200 K. For these temperatures and the boron molar fraction, the density of the boron vapor is: $n_0 \approx 3 \times 10^{22}$ m$^{-3}$. The cooling rate $\dot{T}_0$ is about $6 \times 10^4$ K s$^{-1}$ (according to ref. 22, the flow velocity is about 20 m s$^{-1}$ and the temperature gradient is 3000 K m$^{-1}$ in the region of interest) in the case with hydrogen addition, when BNNTs are produced. Substitution of these parameters into (11) yields the diameter of the boron droplets upon formation of BNNTs of about 20 nm. It is difficult to validate this value experimentally, *in situ* measurements of the droplets diameters amidst the flight, when nanotubes grow on them, would be required. However, validation of this model can be performed by comparing the final size of the boron droplets predicted by (11) with the *ex situ* TEM images of boron droplets with no nanotubes produced in the case without addition of hydrogen (see Fig. 3f in ref. 22). In the no-hydrogen case, the cooling rate was about $10^5$ K s$^{-1}$ (velocity 20 m s$^{-1}$ and the temperature gradient about 5000 K m$^{-1}$). Substitution of this value and $T_{B\_solid}$ in (11) yields a final diameter of boron droplets of about 20 nm (coincidently, the same as for boron droplets with nanotubes grown with the addition of hydrogen). As seen from the TEM image,[22] there were mainly boron particles of 15–20 nm, which is in a good agreement with our theoretical prediction.

The same method can be applied to assess the size of boron droplets in the electric arc reactor for BNNT synthesis.[15] Unfortunately, no quantitative data are available on the boron molar fraction and the gas cooling rate within the nanoparticle growth region in an electric arc in nitrogen for the synthesis of BNNTs. However, for general assessment, analogy with a carbon arc studied in ref. 43 can be employed here: both arcs have similar size and power, in both arcs one of the electrodes ablates, and the evaporated material (boron or carbon) diffuses in the surrounding gas to the nanoparticle growth region. This approach makes sense because the results of (11) are weakly dependent on the input parameters. In ref. 43, simulations predicted coincidently the same parameters as in the ICP system:[22] the molar fraction of the ablated material in the growth region is about 1%, and the cooling rate $\dot{T}_0$ is about $2.5 \times 10^5$ K s$^{-1}$. This yields the diameter of the boron droplets of about 1015 nm. This result is in agreement with the *ex situ* TEM image of the boron droplets with nanotubes grown on them (see Fig. 3 in ref. 15). Again, these estimates provide just an order of magnitude, for more accurate predictions, modeling of the arc in nitrogen for BNNT synthesis is required.

### III.G. Analytical relations for species densities

In the thermodynamic approach, the densities of species are determined *via* minimization of relation (7) with constraints (5) and (6). Note that in (7), the densities of various species are substantially different, by many orders of magnitude. Apparently, species with higher densities have a higher impact on the chemical composition of other species within the system. Having this in mind, relation (7) can be substantially simplified when determining the density of any particular species. For any species of interest, only species with major densities having the same chemical elements need to be considered.

For instance, when considering atomic nitrogen, only diatomic nitrogen $N_2$ needs to be kept in eqn (7) as a dominant nitrogen-containing species. This yields the following relation for the densities of N and $N_2$:

$$\sum_{i\in \mathrm{N},\mathrm{N}_2} N_i\left(kT\left(\ln N_i - \ln\left(\sum_{k\in \mathrm{N},\mathrm{N}_2} N_k\right) + \ln\frac{p}{p_0}\right) + G_i(p_0,T)\right) \rightarrow \min, \tag{12}$$

with the following constraint:

$$N_\mathrm{N} + 2N_{\mathrm{N}_2} = N_\mathrm{N}^{\star}. \tag{13}$$

Here, $N_\mathrm{N}$ is the number of nitrogen atoms, $N_{\mathrm{N}_2}$ is the number of nitrogen diatomic molecules, and $N_\mathrm{N}^{\star}$ is the total number of nitrogen atoms in all species within the system (is constant); $p_0$ = 1 atm is the reference pressure for which the Gibbs energies of formation $G_i^\mathrm{f}$ are determined for various species $i$, as introduced in eqn (2).

The solution of (12) and (13) yields the following relation:

$$\frac{N_{\mathrm{N}_2}\left(N_{\mathrm{N}_2}+N_\mathrm{N}\right)}{N_\mathrm{N}^2} = \frac{p}{p_0}\exp\left(\frac{\Delta G_\mathrm{N}}{RT}\right),$$

where $\Delta G_\mathrm{N} = 2G_\mathrm{N}^\mathrm{f}(p_0,T) - G_{\mathrm{N}_2}^\mathrm{f}(p_0,T)$; $G_\mathrm{N}$ and $G_{\mathrm{N}_2}$ are the energies of formation for N and $N_2$ respectively. Or, in terms of species densities (using relation (8)):

$$\frac{n_{\mathrm{N}_2}\left(n_{\mathrm{N}_2}+n_\mathrm{N}\right)}{n_\mathrm{N}^2} = \frac{p}{p_0}\exp\left(\frac{\Delta G_\mathrm{N}}{RT}\right).$$

This relation is known as the law of mass action[46,83] for a dissociation reaction. Taking into account that $N_2$ is the major component in the mixture within the temperature range considered, and its partial pressure is roughly equal to the total gas pressure $p$, the following relation for the partial pressure of atomic nitrogen is obtained:

$$p_\mathrm{N} = \sqrt{p_0 p}\exp\left(-\frac{\Delta G_\mathrm{N}}{2RT}\right). \tag{14}$$

As for boron, major boron containing species within the mixture is either its atomic gas phase at higher temperatures or its liquid phase at lower temperatures. In order to find the densities of these two species, eqn (7) can be simplified to:

$$N_\mathrm{B}\left(RT\ln\frac{p}{p_0} + G_\mathrm{B}\right) + N_{\mathrm{B,l}}G_{\mathrm{B,l}} \rightarrow \min, \tag{15}$$

with the following constraint:

$$N_\mathrm{B} + N_{\mathrm{B,l}} = N_\mathrm{B}^{\star}. \tag{16}$$

Here, subscripts B and B, l refer to atoms in gas and liquid states respectively. The solution of (15) and (16) yields the following relation for the partial pressure of the atomic boron gas:

$$p_\mathrm{B} = p_0 \min\left(\exp\left(-\frac{\Delta G_\mathrm{B}}{RT}\right), x_{\mathrm{B,max}}\right). \tag{17}$$

Here, $\Delta G_\mathrm{B} = G_\mathrm{B}^\mathrm{f}(p_0,T) - G_{\mathrm{B,l}}^\mathrm{f}(T) + RT$, and $x_{\mathrm{B,max}} \approx 2b_\mathrm{B}$ is the maximum molar fraction of the boron gas (when all boron is in the gas phase). Factor "2" before $b_\mathrm{B}$ is taken into account that boron is mostly present in the atomic form and nitrogen – in form of $N_2$ molecules:

$$x_{\mathrm{B,max}} \approx \frac{N_\mathrm{B}}{N_\mathrm{B}+N_{\mathrm{N}_2}} \approx \frac{N_\mathrm{B}^*}{N_\mathrm{B}^* + N_\mathrm{N}^*/2} = \frac{2b_\mathrm{B}}{1+b_\mathrm{B}} \approx 2b_\mathrm{B}.$$

Relation (17) is similar to a known Clausius–Clapeyron equation for saturation pressure, but formulated in terms of Gibbs free energies.

Knowing the densities and pressures of major nitrogen ($N_2$) and boron (B) gas species allows determining the densities of B–N compound molecules $B_xN_y$. For such molecules, eqn (7) can be written in a simplified form similar to (12), with summation over three species: B, $N_2$ and $B_xN_y$. The following constraints on the species densities should be applied:

$$\begin{aligned} N_\mathrm{B} + xN_{\mathrm{B}_x\mathrm{N}_y} &= N_{\mathrm{B,g}}{}^*, \\ 2N_{\mathrm{N}_2} + yN_{\mathrm{B}_x\mathrm{N}_y} &= N_\mathrm{N}^*. \end{aligned} \tag{18}$$

Here, $N_{\mathrm{B,g}}{}^*$ is the total number of boron atoms in the gas phase, which is determined by condensation of boron and, hence, is conserved on conversion of $N_{\mathrm{B}_x\mathrm{N}_y}$ into other gas species. Both $N_\mathrm{N}^{\star}$ and $N_{\mathrm{B,g}}{}^*$ can be considered constants in (18). The solution of this system in a general case is rather bulky; however, taking into account that $N_{B_xN_y} \ll N_\mathrm{N}^{\star}$ and usually $N_{\mathrm{B,g}}{}^* < N_\mathrm{N}^{\star}$, a compact solution can be written:

$$N_{\mathrm{B}_x\mathrm{N}_y} = (N_\mathrm{B}^*)^x\left(\frac{N_\mathrm{N}^*}{2}\right)^{1-x}\left(\frac{p}{p_0}\right)^{\left(\frac{y}{2}+x-1\right)}\exp\left(-\frac{\Delta G}{RT}\right),$$

or, formulated in terms of partial pressures, taking into account that $N_2$ is the major component in the mixture:

$$p_{\mathrm{B}_x\mathrm{N}_y} = (p_\mathrm{B})^x\frac{p^{\frac{y}{2}}}{p_0{}^{\frac{y}{2}+x-1}}\exp\left(-\frac{\Delta G}{RT}\right). \tag{19}$$

Here, $\Delta G = G_{\mathrm{B}_x\mathrm{N}_y}^\mathrm{f}(p_0,T) - xG_\mathrm{B}^\mathrm{f}(p_0,T) - \frac{y}{2}G_{\mathrm{N}_2}^\mathrm{f}(p_0,T)$. $p_\mathrm{B}$ in (19) can be taken as predicted by (17). For temperatures below the

 

Table 2 Coefficients $A_{B_xN_yH_z}$ and $T_{B_xN_yH_z}$ for various species in eqn (22) for the species densities

| Species, $B_xN_yH_z$ | $A_{B_xN_yH_z}$ | $T_{B_xN_yH_z}$ (K) |
|---|---|---|
| B | 515 000 | 58 800 |
| $B_2$ | 1 962 000 | 81 900 |
| $B_3$ | 238 000 | 74 100 |
| N | 3600 | 58 100 |
| $N_3$ | $2.9 \times 10^{-3}$ | 51 700 |
| BN | 359 000 | 65 000 |
| $B_2N$ | 535 000 | 40 700 |
| H | 1570 | 27 500 |
| BH | 5300 | 44 000 |
| $BH_2$ | 5.2 | 15 400 |
| $BH_3$ | $7.2 \times 10^{-4}$ | 2780 |
| NH | 11.5 | 45 400 |
| $NH_2$ | $7.1 \times 10^{-3}$ | 22 400 |
| $NH_3$ | $9.7 \times 10^{-7}$ | −6100 |

saturation point of boron this yields:

$$p_{B_xN_y} = \frac{p^{\frac{y}{2}}}{p_0^{\frac{y}{2}-1}} \exp\left(-\frac{\Delta\tilde{G}}{RT}\right), \quad (20)$$

where $\Delta\tilde{G} = G^f_{B_xN_y}(p_0, T) - \frac{y}{2}G^f_{N_2}(p_0, T) - xG^f_{B,l}(T) - xRT$.

Eqn (20) can be considered as a generic equation for boron and nitrogen containing species N, BN, $B_2N$, B, $B_2$ and $N_2$ corresponding to different values of $x$ and $y$. Typically, $\Delta\tilde{G}$ has a linear dependence on temperature. In this regard, eqn (20) can be rewritten in the Arrhenius form:

$$p_{B_xN_y} = p^{\frac{y}{2}} p_0^{1-\frac{y}{2}} A_{B_xN_y} \exp\left(-\frac{T_{B_xN_y}}{T}\right). \quad (21)$$

Similar relations can be derived for hydrogen-containing species H, $B_xH_y$ and $N_xH_y$, for temperatures below 3200 K, where $H_2$ is the major hydrogen-containing component (see Fig. 3 and 4). For convenience, let's formulate it in a general form, for species $B_xN_yH_z$ ($x$, $y$ and $z$ can be zero). The relation for the partial pressure as a function of Gibbs free energy change takes a form:

$$p_{B_xN_yH_z} = p^{\frac{y+z}{2}} p_0^{1-\frac{y+z}{2}} \exp\left(-\frac{\Delta\hat{G}}{RT}\right),$$

where $\Delta\hat{G} = G^f_{B_xN_yH_z}(p_0, T) - xG^f_{B,l}(T) - \frac{y}{2}G^f_{N_2}(p_0, T) - \frac{z}{2}G^f_{H_2}(p_0, T) - xRT$.

This yields the following Arrhenius form for the partial pressure of $B_xN_yH_z$ species:

$$p_{B_xN_yH_z} = p^{\frac{y+z}{2}} p_0^{1-\frac{y+z}{2}} A_{B_xN_yH_z} \exp\left(-\frac{T_{B_xN_yH_z}}{T}\right), \quad (22)$$

The values of coefficients $A_{B_xN_yH_z}$ and $T_{B_xN_yH_z}$ for various species are summarized in Table 2.

The pressures of B atoms, $N_2$, BN and $B_2N$ molecules obtained with formulas (14), (17) and (19) are plotted in Fig. 7 as functions of temperature, in comparison with the results of the full thermodynamic solution for the B–N mixture. As seen from the figure, at temperatures above the point of solid BN formation, simple algebraic relations (14), (17) and (19) provide pretty accurate values without the need to perform numerical minimization of relation (7). This enables quick analysis of the mixture composition and determination of the species present when BNNTs and other BN structures start to form.

## IV. Conclusions

Calculations of the equilibrium chemical composition for the B–N mixture with and without addition of hydrogen at 1 atm and 10 atm in the temperature range between 1000 K and 6000 K were performed using a thermodynamic approach. A broad set of species was considered including BN, $B_2N$ and $BN_2$ gas phase molecules, liquid boron and solid BN. The latter allowed accounting for condensation of boron and determining conditions at which the formation of solid BN structures take place, which can be interpreted as conditions for the growth of

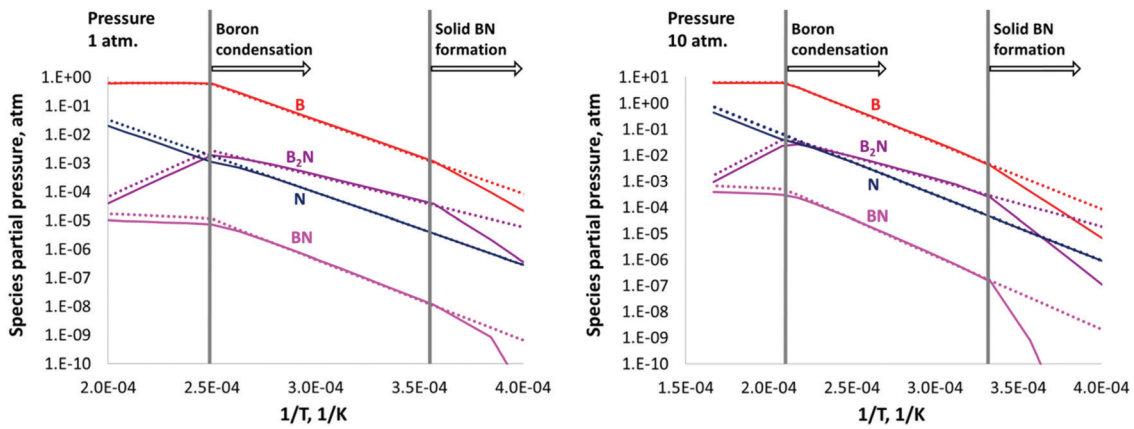


Fig. 7 Partial pressures of the selected species obtained using algebraic relations (14), (17) and (19) as functions of temperature (dotted lines), in comparison with the results of full thermodynamic modeling of the B–N mixture (solid lines). 45% boron and 55% nitrogen within the mixture, two pressures are considered. Good agreement between the full modeling results and analytical solutions is observed for temperatures higher than the point of solid BN formation.

BNNTs. The thermodynamic calculations predict that in a cooling mixture, boron condenses at first providing seed particles for the growth of BNNTs, supporting the "root growth" mechanism. It was shown that condensation of boron has a drastic effect on the gas phase composition yielding reduction of boron-containing species densities by several orders of magnitude at temperatures corresponding to the formation of boron liquid (droplets) and BNNTs. This effect was not considered in previous thermodynamic studies of B–N mixtures and should be taken into account when studying conditions for the growth of BNNTs.

The results of the thermodynamic calculations have shown that $B_2N$ molecules have the highest density among nitrogen-containing species, after $N_2$, when BNNTs grow on the surface of boron droplets. Unlike $B_2N$ molecules, $N_2$ has a high dissociation energy and can hardly dissociate on a boron surface in order to contribute to the formation of the periodic B–N structure within BNNT. Hence, $B_2N$ molecules can be suggested as major sources of nitrogen and major building molecules for the formation and growth of BNNTs. These predictions are supported by the experimental results obtained by our OES measurements during the laser ablation of the boron-rich target. Atomic nitrogen can provide some contribution to the growth as well. Other nitrogen-containing species have much lower densities and cannot have a substantial impact on the growth of BNNTs.

The results of the thermodynamic calculations were also verified by qualitative comparison to spectroscopic measurements of the gas composition at several locations within the ICP plasma reactor of ref. 22. The measured spectral line intensities of several species (N, $N_2$, NH, B, BH, H, BN, and $H_2$) at three locations in the ICP plasma reactor qualitatively agree with the predictions of the thermodynamic calculations.

The effect of the pressure increase from 1 atm to 10 atm on the gas composition was studied. It was shown that because the density of boron gas is determined merely by the saturation curve and does not depend on the background pressure, the densities of N, BN and $B_2N$ molecules increase proportionally to the square root of pressure. These results suggest that precursors for formation of BNNTs remain the same ($B_2N$ molecules and N atoms), and the enhanced production yield and purity of BNNTs observed in ref. 17 and 20 at higher pressures can be attributed to the increase of densities of these precursors.

Convenient analytical relations in the Arrhenius form (22) were derived to describe species densities at various pressures and temperatures higher than point of solid BN formation. The values of coefficients for the Arrhenius expression for various species were provided.

Ref. 21 and 22 observed enhanced BNNT production with hydrogen addition. Our analysis shows that formation of $NH_3$ molecules at temperatures of BNNT growth might be responsible for this effect. Nitrogen atoms react fast with abundant $H_2$ molecules to form $NH_2$ and then $NH_3$ species, instead of just recombining back to inert $N_2$ molecules in the no-hydrogen case. These $NH_3$ molecules can provide additional nitrogen to boron droplets and hence enhance the BNNT growth.

We calculate the size of the boron droplets where BNNTs grow. The boron gas density, temperature and flow velocity were taken from the fluid modeling.[22,43] Good agreement between our simulation results and those observed in *ex situ* TEM photos[15,22] for the droplet size was obtained. It was shown that the initial fraction of boron in the system does not affect the composition of the gas mixture when BNNTs grow, because most of boron condenses into liquid droplets (though the initial fraction of boron affects the size of the boron droplets on which the BNNTs grow, see eqn (10)).

## Conflicts of interest

There are no conflicts to declare.

## Note from RSC Publishing

This article was originally published with incorrect page numbers. This is the corrected, final version. The Royal Society of Chemistry apologises for these errors and any consequent inconvenience to authors and readers.

## Appendix A: details of the experimental setup for laser ablation of boron-rich targets and OES measurements

Laser ablation is driven by an Nd:Yag laser (Surelite III-10), equipped with second and third harmonic generators. The laser produced pulses of 1064 nm wavelength at a frequency of 10 Hz, which are converted to 355 nm, using a frequency conversion unit. The emerging laser has a full-width-at-half-maximum (FWHM) duration of $\sim$7 ns. The laser beam was guided into the investigation area and focused on the target with lens ($f$ = 300 mm). The target is a boron-nitride (BN) tablet, having a diameter of 25 mm and a height of 5 mm. The BN target was held in a 3D-printed pedestal, which in turn was connected to a rotation motor. Fast rotation of the target prevents the dipping of the laser into the target. The resulting ablation plume is imaged with a lens on the entrance of the imaging spectrometer (iHoriba 550). The entrance slit of the spectrometer was set to a width of 50 microns and a spectrometer grating of 1200 groves per mm was employed to diffuse the light. An iCCD camera (PI-MAX 3, 1024 $\times$ 1024 pixel CCD) is connected to the exit port of the spectrometer for detection. A Dove prism located between the lens and the spectrometer slit rotates the image by 90°. In this fashion the ablation plume was imaged using the iCCD vertically: the target was on the top of the CCD, the plume was extended from the top to bottom and the horizontal direction on the iCCD corresponds to different wavelengths.

## Appendix B: assessment of the plasma decay time at the surfaces of boron droplets

In ionized gas, particle coagulation might be affected by their charges, as shown for example in ref. 79 and 80. However, in

 

these references, low pressure high temperature (5 eV) plasmas were considered, with the ionization rate being sufficient to compensate the loss of charge particles due to the ion (positive ion-electron) recombination at the droplet surfaces and maintain the plasma. In atmospheric (and higher) pressure nanosynthesis reactors, at the temperature of boron condensation and coagulation (about 0.3 eV), the ionization rate is much lower, and plasma decay on the surfaces of boron droplets plays an important role.

At these temperatures, the effects of photo- and thermal emission on the particle charges are negligible. The droplets are charged negatively due to bombardment by plasma electrons. These negatively charged droplets attract ions that recombine on their surfaces neutralizing the droplet charge (boron is conductive in the liquid state[84]). The volumetric ion recombination rate at the droplet surfaces can be assessed as:

$$r_r \geq \pi d^2 n_d n_i \sqrt{\frac{2kT}{m_B}}. \quad \text{(B1)}$$

Here, $d$ is the droplets' dimeter, $n_d$ and $n_i$ are the densities of boron droplets and ions, respectively, $m_B$ is the mass of the boron ion. This is an estimate from below; the effect of the droplet charge is neglected for simplicity (the negative charge of the droplets only increases the recombination rate).

For convenience, the density and diameter of the boron droplets can be linked *via* mass conservation:

$$n_d = 8 n_0 r_0^3 / d^3. \quad \text{(B2)}$$

Here $n_0 \approx 3 \times 10^{22}$ m$^{-3}$ is the density of the boron atoms before the condensation, and $r_0 \approx 1.2 \times 10^{-10}$ m is the Wigner–Seitz radius (see Section III.F).

Substitution of this relation into eqn (B1) yields for the plasma decay time:

$$t_{decay} \leq \frac{d}{8\pi n_0 r_0^3} \sqrt{\frac{m_B}{2kT}}. \quad \text{(B3)}$$

According to this expression, plasma decays quite fast in the beginning of the coagulation process, when the droplets are small. For 1 nm droplets, the plasma decay time is $t_{decay} \leq 5 \times 10^{-7}$ s. This is considerably faster than the coagulation time ($10^{-5}$ s for the droplets to reach 1 nm in diameter, according to eqn (10) from Section III.F).

The volumetric ionization rate is given by:

$$r_i = k_i n_e n_B. \quad \text{(B4)}$$

Here, $k_i$ is the rate coefficient, $n_e$ and $n_B$ are the densities of the electrons and boron atoms. For boron at an electron temperature of 0.3 eV, the rate coefficient is $k_i = 10^{-19}$ m$^3$ s$^{-1}$, calculated using formula (59) from ref. 85 for step-ionization of an atom at low temperatures. Taking into account that $n_e < n_i$ (the negative charge from plasma is partially accumulated on the droplets) and $n_B < n_0$, estimate from below for the ionization time is:

$$t_{ioniz} \geq (k_i n_0)^{-1} = 3 \times 10^{-4} \text{ s}. \quad \text{(B5)}$$

This is much larger than the recombination time ($t_{decay} \leq 5 \times 10^{-7}$ s, as discussed earlier); hence, the effect of ionization in the plasma is negligible.

From these assessments it is clear that as soon as the droplets appear, the plasma will virtually immediately disappear (much faster than solid BN formation initiates after about 0.01 s). The negative charge will be removed from the droplets *via* recombination of ions, and the coagulation will take place for uncharged droplets, as described in Section III.F.

## Appendix C: applicability of the thermodynamic approach to model the nanosynthesis systems

Thermodynamics is a useful theoretical tool for determining the equilibrium composition of complex reacting systems of multiple components without the need to go into the details of a chemical mechanism that leads a system to this state. The latter would require quite extensive calculations of chemical reaction rates among various species within a system; the rate coefficients for some of these reactions are often unknown.

If physical timescale for variation of external conditions (temperature, pressure *etc.*) is greater than a chemical timescale at which the mixture composition adapts to the condition change, then the system can be considered to be in equilibrium at each timeframe, and the thermodynamic approach is valid. If the rates of some species formation/destruction are low, then the densities of these species can deviate from an equilibrium solution.

The aim of this paper is to find out what gas phase species bring nitrogen to the surfaces of boron droplets when BNNTs grow on them. Molecular nitrogen ($N_2$), the most abundant species in the system, cannot be directly incorporated into the periodic B–N structure of BNNTs. The $N_2$ molecules have a strong bond (9.8 eV) and do not dissociate on boron droplet surfaces.[26] However, the $N_2$ molecules can be efficiently dissociated in a gas volume *via* stepwise excitation of its vibrational degree of freedom[86,87] through collisions with gas phase species, ultimately resulting in bond breakage. Atomic nitrogen released in this process can participate in the growth of BNNTs by either directly impinging boron droplets or *via* recombination with other gas phase species to form molecules with relatively low binding energies that can release atomic nitrogen (or a B–N couple) at a boron droplet surface.

Thermodynamic modeling predicts that $B_2N$ and then (at a lower temperature) $NH_3$ molecules have the highest density among nitrogen-containing species in a temperature range corresponding to BNNT growth. BN and NH molecules, which has been suggested in ref. 22 as potential channels to provide nitrogen for BNNTs, have, according to the thermodynamic results, noticeable densities only at higher temperatures (above 4000 K) which then rapidly decay when temperatures decrease to the values corresponding to BNNT growth ($\leq$2800 K).

In order to verify whether the thermodynamic method can be applied to describe nano-synthesis systems, the timescales for $B_2N$ and $NH_3$ formation and for BN and NH destruction

(dissociation) have to be compared to a timescale of temperature variation in the system. The latter is about 0.01 s in the ICP/arc discharge reactors (the temperature decay rate is $10^5$ K $s^{-1}$, and temperature variation scale is 1000 K).

For the sake of simplicity, when assessing the timescale of $B_2N$ and $NH_3$ formation, only one chemical pathway for each of these molecules will be considered. Additional formation mechanisms can only increase the formation (production) rates (reduce formation time).

The pathway for $B_2N$ molecule formation is:

$$N_2 + M \rightarrow N + N + M;$$

$$N + B + M \rightarrow BN + M;$$

$$B + BN + M \rightarrow B_2N + M.$$

The pathway for $NH_3$ molecule formation is:

$$N + H_2 + M \rightarrow NH_2 + M;$$

$$NH_2 + H_2 \rightarrow NH_3 + H.$$

$N_2$ and $H_2$ molecules and B atoms are the major nitrogen- and boron-containing components within the system, present in abundance. "M" represents all components in the system.

The production rate of a final product ($B_2N$/$NH_3$) is a minimum of the production rates at each step of a chemical mechanism. The assessments of the production rates are summarized in Tables 3 and 4. The reaction rates for BN and $B_2N$ molecule recombination were assessed using a simple theory, formula (6.27) from ref. 87.

The density of the $B_2N$ molecules is at its highest level at 4000 K (see Fig. 3); the production rates in Table 3 were calculated for this temperature. As it can be seen from the table, the slowest reaction in the $B_2N$ formation mechanism is the dissociation of nitrogen (recombination reactions to form BN and then $B_2N$ are faster). This reaction might be a "bottleneck" limiting the formation of $B_2N$ molecules. The production rate of $4 \times 10^{22}$ $m^{-3}$ $s^{-1}$ determined by the $N_2$ dissociation (two N atom are produced per each dissociation event) is sufficient to raise the density of $B_2N$ molecules to $4 \times 10^{20}$ $m^{-3}$ (molar fraction $2 \times 10^{-4}$) on a timeframe of 0.01 s (during which the temperature in the system is close to the considered value). This density value is about five times lower than the peak density predicted by the thermodynamics, but it is considerably higher than the density at the temperature when BNNTs grow. Thereby, for a mixture cooling in a reactor, the "peak" of the $B_2N$ density profile can be slightly "cut off" on the top, but the density at the BNNTs growth should agree with the thermodynamics predictions.

Note that, in the nanosynthesis reactors, the mixture comes from a hot zone (temperatures above 6000 K) where nitrogen is highly dissociated. Hence, there might be already sufficient amounts of atomic nitrogen in the system. With this, the system might "bypass" the nitrogen dissociation bottleneck and go straight to the formation of BN and $B_2N$ molecules *via* fast recombination reactions. In this regard, even the peak $B_2N$ density value might be in a good agreement with the thermodynamic prediction. This question is not important from the standpoint of BNNT growth but might be interesting from a theoretical point of view. The detailed chemical kinetic calculations accounting for multiple simultaneous reactions would be required to answer this question. This is a complex task additionally complicated by the unavailability of rate coefficients for many reactions. Such considerations are out of the scope of this paper.

According to the thermodynamic prediction (Fig. 3), $NH_3$ molecules become the major nitrogen-containing gas-phase component at the temperature of BNNT formation (2800 K), with exponentially raising density (with the temperature decay). As seen from Table 3, the nitrogen dissociation reaction is the slowest one in the $NH_3$ production pathway at this temperature. However, since a gas mixture comes from a hotter reactor region, it already has a decent amount of atomic nitrogen. According to the thermodynamics results (Fig. 3), the amount of atomic nitrogen in the mixture at a temperature of 3000 K (right before $NH_3$ molecules are produced) exceeds the amount of $NH_3$ molecules produced at 2800 K. Within the mixture, the nitrogen atoms recombine with each other (to form $N_2$ molecules) and with $H_2$ (to form $NH_2$ molecules with their further transformation to $NH_3$). The density of $H_2$ molecules is by many orders of magnitude higher than the density of the N atoms at this temperature. The rate of the $NH_2 + H_2$ chemical reaction leading to $NH_3$ molecule formation is very high (Table 4). Thereby, almost all atomic nitrogen should be incorporated, very quickly, in $NH_3$ molecules, which should

Table 3 Production rates within a pathway for $B_2N$ molecule formation

| Chemical reaction | Temp. (K) | Rate coef. | Ref. | Reactants densities, $m^{-3}$ (according to thermod.) | Production rate ($m^{-3}$ $s^{-1}$) |
|---|---|---|---|---|---|
| $N_2 + M \rightarrow N + N + M$ | 4000 | $10^{-26}$ ($m^3$ $s^{-1}$) | 88 | $N_2$: $10^{24}$, B: $10^{24}$, N: $2 \times 10^{21}$, BN: $10^{19}$, M: $2 \times 10^{24}$ | $4 \times 10^{22}$ |
| $N + B + M \rightarrow BN + M$ | | $10^{-44}$ ($m^6$ $s^{-1}$) | 87 | | $4 \times 10^{25}$ |
| $B + BN + M \rightarrow B_2N + M$ | | $10^{-44}$ ($m^6$ $s^{-1}$) | 87 | | $2 \times 10^{23}$ |

Table 4 Production rates within a pathway for $NH_3$ molecule formation

| Chemical reaction | Temp. (K) | Rate coef. | Ref. | Reactants densities, $m^{-3}$ (according to thermod.) | Production rate ($m^{-3}$ $s^{-1}$) |
|---|---|---|---|---|---|
| $N_2 + M \rightarrow N + N + M$ | 2800 | $2 \times 10^{-31}$ $m^3$ $s^{-1}$ | 88 | $N_2$: $10^{24}$, $H_2$: $10^{24}$, $NH_2$: $10^{18}$, M: $2 \times 10^{24}$ | $8 \times 10^{17}$ |
| $N + H_2 + M \rightarrow NH_2 + M$ | | $10^{-44}$ $m^6$ $s^{-1}$ | 89 | | $2 \times 10^{24}$ |
| $NH_2 + H_2 \rightarrow NH_3 + H$ | | $10^{-17}$ $m^3$ $s^{-1}$ | 90 | | $10^{25}$ |

 

Table 5 Rates and timescales of molecule dissociation

| Chemical reaction | Temp. (K) | Rate coefficient ($m^3$ $s^{-1}$) | Ref. | Reactants densities ($m^{-3}$) | Characteristic time (s) |
|---|---|---|---|---|---|
| NH + M→ N + H + M | 3000 | $10^{-21}$ | 91 | M: $2 \times 10^{24}$ | $5 \times 10^{-4}$ |
| BN + M→ B + N + M | | $10^{-21}$ | 87 | M: $2 \times 10^{24}$ | $5 \times 10^{-4}$ |

reach the densities predicted by the thermodynamics on a timescale of $10^{-5}$ s. This means, it is much faster than the temperature variation timescale. In other words, the presence of hydrogen in the system should prevent the recombination of N atoms into $N_2$ molecules due to their much faster recombination with abundant molecular $H_2$ to form $NH_3$ molecules. These $NH_3$ molecules might serve as efficient sources of nitrogen enhancing the growth of BNNTs.

The rates and timescales of the BN and NH dissociation are shown in Table 5. The dissociation rate coefficient for the BN molecule was calculated using an equilibrium constant and formula (6.27) from ref. 87 for a reversed reaction. As seen from the table, the dissociation of these molecules is much faster (timescale $5 \times 10^{-4}$ s) than the temperature variation (timescale 0.01 s). Thereby, thermodynamic prediction should accurately predict the densities of these molecules at temperatures of BNNT growth, showing superior densities of $B_2N$ and $NH_3$ molecules.

## Acknowledgements

The authors would like to thank Dr Predrag Krstic (Stony Brook University), Dr Longtao Han (Stony Brook University), Dr Rachel Selinsky (Princeton University), Dr Roberto Car (Princeton University), Dr Biswajit Santra (Princeton University) and Dr Andrei Khodak (PPPL) for fruitful discussions. The thermodynamic modeling was supported by the US Department of Energy (DOE), Office of Science, Fusion Energy Sciences. The laser ablation experiments and nanoparticle growth calculations were supported by the US DOE, Office of Science, Basic Energy Sciences, Materials Sciences and Engineering Division.

## References

1 N. G. Chopra and A. Zettl, Measurement of the elastic modulus of a multi-wall boron nitride nanotube, *Solid State Commun.*, 1998, **105**, 297–300.
2 P. Arenal, M.-S. Wang, Z. Xu, A. Loiseau and D. Golberg, Young modulus, mechanical and electrical properties of isolated individual and bundled single-walled boron nitride nanotubes, *Nanotechnology*, 2011, **22**, 265704.
3 C. Chang, A. Fennimore, A. Afanasiev, D. Okawa, T. Ikuno, H. Garcia, D. Li, A. Majumdar and A. Zettl, Isotope effect on the thermal conductivity of boron nitride nanotubes, *Phys. Rev. Lett.*, 2006, **97**, 085901.
4 C. H. Lee, J. Drelich and Y. K. Yap, Superhydrophobicity of boron nitride nanotubes grown on silicon substrates, *Langmuir*, 2009, **25**, 4853–4860.
5 M. Zheng, X. Chen, I.-T. Bae, C. Ke, C. Park, M. W. Smith and K. Jordan, Radial mechanical properties of single-walled boron nitride nanotubes, *Small*, 2012, **8**, 116–121.
6 A. Rubio, J. L. Corkill and M. L. Cohen, Theory of graphitic boron nitride nanotubes, *Phys. Rev. B: Condens. Matter Mater. Phys.*, 1994, **49**, 5081–5084.
7 N. Berseneva, A. V. Krasheninnikov and R. M. Nieminen, Mechanisms of postsynthesis doping of boron nitride nanostructures with carbon from first-principles simulations, *Phys. Rev. Lett.*, 2011, **107**, 35501.
8 X. Wei, M.-S. Wang, Y. Bando and D. Golberg, Post-synthesis carbon doping of individual multiwalled boron nitride nanotubes via electron-beam irradiation, *J. Am. Chem. Soc.*, 2010, **132**, 13592.
9 M. El Khalifi, J. Bentin, E. Duverger, T. Gharbi, H. Boulahdour and F. Picaud, Encapsulation capacity and natural payload delivery of an anticancer drug from boron nitride nanotube, *Phys. Chem. Chem. Phys.*, 2016, **18**, 24994.
10 V. Raffa, C. Riggio, M. W. Smith, K. C. Jordan, W. Cao and A. Cuschieri, BNNT-mediated irreversible electroporation: its potential on cancer cells, *Technol. Cancer Res. Treat.*, 2012, **11**, 459–465.
11 M. E. Suk, A. V. Raghunathan and N. R. Aluru, Fast reverse osmosis using boron nitride and carbon nanotubes, *Appl. Phys. Lett.*, 2008, **92**, 133120.
12 L. Liang, J.-C. Li, L. Zhang, Z. Zhang, J.-W. Shen, L. Li and J. Wu, Computer simulation of water desalination through boron nitride nanotubes, *Phys. Chem. Chem. Phys.*, 2017, **19**, 30031–30038.
13 C. H. Lee, S. Bhandari, B. Tiwari, N. Yapici, D. Zhang and Y. K. Yap, Boron nitride nanotubes: recent advances in their synthesis, functionalization, and applications, *Molecules*, 2016, **21**, 922.
14 J. Cumings and A. Zettl, Mass-production of boron nitride double-wall nanotubes and nanococoons, *Chem. Phys. Lett.*, 2000, **316**, 211–216.
15 Y. W. Yeh, Y. Raitses, B. E. Koel and N. Yao, Stable synthesis of few-layered boron nitride nanotubes by anodic arc discharge, *Sci. Rep.*, 2017, **7**, 3075.
16 R. Arenal, O. Stephan, J.-L. Cochon and A. Loiseau, Root-growth mechanism for single-walled boron nitride nanotubes in laser vaporization technique, *J. Am. Chem. Soc.*, 2007, **129**, 16183–16189.
17 M. W. Smith, K. C. Jordan, C. Park, J.-W. Kim, P. T. Lillehei, R. Crooks and J. S. Harrison, Very long single-and few-walled boron nitride nanotubes *via* the pressurized vapor/condenser method, *Nanotechnology*, 2009, **20**, 505604.
18 M. Xie, J. Wang and Y. K. Yap, Mechanism for low temperature growth of boron nitride nanotubes, *J. Phys. Chem. C*, 2010, **114**, 16236.

19 A. L. Tiano *et al.*, *Boron nitride nanotube: synthesis and applications*, in Proc. SPIE 9060, Nanosensors, Biosensors, and Info-Tech Sensors and Systems, 2014, p. 906006, DOI: 10.1117/12.2045396; https://ntrs.nasa.gov/archive/nasa/casi.ntrs.nasa.gov/20140004051.pdf.
20 A. Fathalizadeh, T. Pham, W. Mickelson and A. Zettl, Scaled synthesis of boron nitride nanotubes, nanoribbons, and nanococoons using direct feedstock injection into an extended-pressure, inductively-coupled thermal plasma, *Nano Lett.*, 2014, **14**, 4881–4886.
21 K. S. Kim, C. T. Kingston, A. Hrdina, M. B. Jakubinek, J. Guan, M. Plunkett and B. Simard, Hydrogen-catalyzed, pilot-scale production of small-diameter boron nitride nanotubes and their macroscopic assemblies, *ACS Nano*, 2014, **8**, 6211–6220.
22 K. S. Kim, M. Couillard, H. Shin, M. Plunkett, D. Ruth, C. T. Kingston and B. Simard, Role of hydrogen in high-yield growth of boron nitride nanotubes at atmospheric pressure by induction thermal plasma, *ACS Nano*, 2018, **12**, 884–893.
23 L. Wang, T. Li, X. Long, X. Wang, Y. Xu and Y. Yao, Bimetallic catalytic growth of boron nitride nanotubes, *Nanoscale*, 2017, **9**, 1816–1819.
24 S. E, C. Li, T. Li, R. Geng, Q. Li, W. Lu and Y. Yao, Ammonium-tungstate-promoted growth of boron nitride nanotubes, *Nanotechnology*, 2018, **29**, 195604.
25 K. S. Kim, M. J. Kim, C. Park, C. C. Fay, S.-H. Chu, C. T. Kingston and B. Simard, Scalable manufacturing of boron nitride nanotubes and their assemblies: a review, *Semicond. Sci. Technol.*, 2017, **32**, 013003.
26 B. Santra, H.-Y. Ko, Y.-W. Yeh, F. Martelli, I. Kaganovich, Y. Raitses and R. Car, Root-growth of boron nitride nanotubes: experiments and *ab initio* simulations, *Nanoscale*, 2018, **10**, 22223, DOI: 10.1039/C8NR06217J.
27 P. S. Krstic, L. Han, S. Irle and H. Nakai, Simulations of the synthesis of boron-nitride nanostructures in a hot, high pressure gas volume, *Chem. Sci.*, 2018, **9**, 3803–3819.
28 U. R. Kortshagen, R. M. Sankaran, R. N. Pereira, S. L. Girshick, J. J. Wu and E. S. Aydil, Nonthermal plasma synthesis of nanocrystals: fundamental principles, materials, and applications, *Chem. Rev.*, 2016, **116**, 11061.
29 K. Ostrikov, E. C. Neyts and M. Meyyappan, Plasma nanoscience: from nano-solids in plasmas to nano-plasmas in solids, *Adv. Phys.*, 2013, **62**, 113–224, DOI: 10.1080/00018732.2013.808047.
30 K. Ostrikov, Plasma nanoscience: from nature's mastery to deterministic plasma-aided nanofabrication, *IEEE Trans. Plasma Sci.*, 2007, **35**, 127–136.
31 K. Ostrikov, *Plasma nanoscience: basic concepts and applications of deterministic nanofabrication*, Wiley, 2008, p. 563.
32 A. L. Tiano, C. Park, J. W. Lee, H. H. Luong, L. J. Gibbons, S.-H. Chu, S. Applin, P. Gnoffo, S. Lowther and H. J. Kim *et al.*, Boron nitride nanotube: synthesis and applications, in *Proc. SPIE 9060, Nanosensors, Biosensors, and Info-Tech Sensors and Systems*, ed. V. K. Varadan, SPIE, San Diego, CA, USA, 2014, vol. 9060.
33 P. Fauchais, M. I. Boulos and E. Pfender, *Thermal plasmas—fundamentals and applications*, Plenum, New York, 1994, vol. 1.
34 Y. Lwin, Chemical equilibrium by Gibbs energy minimization on spreadsheets, *Int. J. Engng. Ed.*, 2000, **16**, 335–339.
35 H. Maecker and H.-P. Popp, *The electric arc: the physics of stationary gas discharges near thermal equilibrium*, H. Popp Matlab GmbH, Berg, Germany, 2009, ISBN 978-3-00-023602-0.
36 C. Dutouquet, S. Acquaviva and J. Hermann, Detection of boron nitride radicals by emission spectroscopy in a laser-induced plasma, *Spectrochim. Acta, Part B*, 2001, **56**, 629–635.
37 J. Radic-Peric, Thermodynamic modelling of boron nitride formation in thermal plasma, *Mater. Sci. Forum*, 2006, **518**, 349–354.
38 J. Radić-Perić and N. Pantelić, Thermodynamical modeling of silicon carbide synthesis in thermal plasma, *J. Therm. Anal. Calorim.*, 2003, **72**, 35–45.
39 NIST-ANAF Thermochemical tables, Journal of Physical and Chemical Reference Data, Fourth Edition, Malcolm W. Chase, Jr., 1998.
40 J. M. L. Martin, J. P. François and R. Gijbels, *Ab initio* study of boron, nitrogen, and boron–nitrogen clusters. I. Isomers and thermochemistry of $B_3$, $B_2N$, $BN_2$, and $N_3$, *J. Chem. Phys.*, 1989, **90**, 6469–6485.
41 G. Cota-Sanchez, G. Soucy, A. Huczko and H. Lange, Induction plasma synthesis of fullerenes and nanotubes using carbon black–nickel particles, *Carbon*, 2005, **43**, 3153–3166.
42 V. Vekselman, A. Khrabry, I. Kaganovich, B. Stratton, R. S. Selinsky and Y. Raitses, Quantitative imaging of carbon dimer precursor for nanomaterial synthesis in the carbon arc, *Plasma Sources Sci. Technol.*, 2018, **27**, 025008.
43 S. Yatom, A. Khrabry, J. Mitrani, A. Khodak, I. Kaganovich, V. Vekselman, B. Stratton and Y. Raitses, Synthesis of nanoparticles in carbon arc: measurements and modeling, *MRS Commun.*, 2018, **8**, 842–849.
44 S. Dhar, V. K. Kumar, T. H. Choudhury, S. A. Shivashankar and S. Raghavan, Chemical vapor deposition of MoS2 layers from Mo–S–C–O–H system: thermodynamic modeling and validation, *Phys. Chem. Chem. Phys.*, 2016, **18**, 14918.
45 K. C. Kim, M. D. Allendorf, V. Stavilab and D. S. Sholl, Predicting impurity gases and phases during hydrogen evolution from complex metal hydrides using free energy minimization enabled by first-principles calculations, *Phys. Chem. Chem. Phys.*, 2010, **12**, 9918–9926.
46 P. Andre, M. Abbaoui, R. Bessege and A. Lefort, Comparison between Gibbs free energy minimization and mass action law for a multitemperature plasma with application to nitrogen, *Plasma Chem. Plasma Process.*, 1997, **17**, 207–217.
47 H. B. Callen, *Thermodynamics*, John Wiley, New York, 1960.
48 D. Kondepudi and I. Prigogine, *Modern Thermodynamics: From Heat Engines to Dissipative Structures*, Wiley, 1998.
49 V. A. Lubarda, On the Gibbs energy and chemical potentials of an ideal gas mixture. The montenegrin academy of sciences and arts, *Proceedings of the section of natural sciences*, 18 (2009), UDK 539.319.
50 S. J. La Placa, P. A. Roland and J. J. Wynne, Boron clusters ($B_n$, $n$ = 2–52) produced by laser ablation of hexagonal boron nitride, *Chem. Phys. Lett.*, 1992, **190**, 163–168.

 

51 L. Andrews, P. Hassanzazadeh, T. R. Burkholder and J. M. L. Martin, Reactions of pulsed laser produced boron and nitrogen atoms in a condensing argon stream, *J. Chem. Phys.*, 1993, **98**, 922–931.
52 K. R. Asmis, T. R. Taylor and D. M. Neumark, Anion photoelectron spectroscopy of small boron nitride clusters: adiabatic detachment energies and vibrational frequencies of low-lying electronic states in $B_2N$ and $B_3N$, *Eur. Phys. J. D*, 1999, **9**, 257–261.
53 P. Cias, M. Araki, A. Denisov and J. P. Mayer, Gas phase detection of cyclic $B_3$: $2^2E - X^2A_1$ electronic origin band, *J. Chem. Phys.*, 2004, **121**, 6776–6778.
54 http://gaussian.com/glossary/g86/.
55 W. Z. Wang, M. Z. Rong, A. B. Murphy, Y. Wu, J. W. Spencer, J. D. Yan and M. T. C. Fang, Thermophysical properties of carbon–argon and carbon–helium plasmas, *J. Phys. D: Appl. Phys.*, 2011, **44**, 355207.
56 B. deB. Darwent, *Bond dissociation energies in simple molecules*, US National Bureau of Standards, 1970.
57 J. M. L. Martin, J. P. Francois and R. Gijbels, *Ab initio* spectroscopy and thermochemistry of the BN molecule, *Z. Phys. D: At., Mol. Clusters*, 1991, **21**, 47–55.
58 J. M. L. Martin, T. J. Lee, G. E. Scuseria and P. R. Taylor, Ab initio multireference study of the BN molecule, *J. Chem. Phys.*, 1992, **97**, 6549–6556.
59 K. A. Peterson, Accurate multireference configuration interaction calculations on the lowest 1Σ+ and 3Π electronic states of C2, CN+, BN, and BO+, *J. Chem. Phys.*, 1995, **102**, 262–277.
60 Y. R. Luo, *Comprehensive handbook of chemical bond energies*, CRC Press, Boca Raton, FL, 2007.
61 B. M. Smirnov, *Cluster processes in gases and plasmas*, Wiley-VCH Verlag Gmbh & Co. KgaA, 2010.
62 Z. H. Li, D. Bhatt, N. E. Schultz, J. I. Siepmann and D. G. Truhlar, Free Energies of Formation of Metal Clusters and Nanoparticles from Molecular Simulations: $Al_n$ with $n$ = 2–60, *J. Phys. Chem. C*, 2007, **111**, 16227–16242.
63 S. M. Kathmann, G. K. Schenter, B. C. Garrett, B. Chen and J. I. Siepmann, Thermodynamics and kinetics of nanoclusters controlling gas-to-particle nucleation, *J. Phys. Chem. C*, 2009, **113**, 10354–10370.
64 S. Panda and S. E. Pratsinis, Modeling the synthesis of aluminum particles by evaporation-condensation in an aerosol flow reactor, *Nanostruct. Mater.*, 1995, **5**, 755–767.
65 A. Prakash, A. P. Bapat and M. R. Zachariah, A Simple Numerical Algorithm and Software for Solution of Nucleation, Surface Growth, and Coagulation Problems, *Aerosol Sci. Technol.*, 2003, **37**, 892–898.
66 S. A. Davari and D. Mukherjee, Kinetic monte carlo simulation for homogeneous nucleation of metal nanoparticles during vapor phase synthesis, *AIChE J.*, 2018, **64**, 18–28.
67 M. Tacu, A. Khrabry and I. D. Kaganovich, Analytical formula for cluster diameter and its dispersion at the end of nucleation stage, 2019, https://arxiv.org/pdf/1903.12268.pdf.
68 L. Han. *Synthesis of boron-nitride nanomaterials in plasma volume*, PhD thesis, Stony Brook Univ., NY, USA, 2018, p. 188.
69 L. Han and P. Krstić, A path for synthesis of boron-nitridenanostructures in volume of arc plasma, *Nanotechnology*, 2017, **28**, 07LT01, DOI: 10.1088/1361-6528/aa5653.
70 C. H. Lee, J. Wang, V. K. Kayatsha, J. Y. Huang and Y. K. Yap, Effective growth of boron nitride nanotubes by thermal chemical vapor deposition, *Nanotechnology*, 2008, **19**, 455605.
71 C. Tang, Y. Bando, T. Sato and K. Kurashima, A novel precursor for synthesis of pure boron nitride nanotubes, *Chem. Commun.*, 2002, 1290–1291.
72 J. M. Modak, Haber process for ammonia synthesis, *Resonance*, 2002, **7**, 69.
73 J. H. Yaoa, C. Shangb, K. F. Aguey-Zinsoua and Z. X. Guo, Desorption characteristics of mechanically and chemically modified $LiNH_2$ and ($LiNH_2$ + LiH), *J. Alloys Compd.*, 2007, **432**, 277–282.
74 A. Kramida, Yu. Ralchenko, J. Reader and NIST ASD Team, (2018), NIST Atomic Spectra Database (ver. 5.5.6), [Online], National Institute of Standards and Technology, Gaithersburg, MD, available: https://physics.nist.gov/asd [2018, August 13].
75 K. P. Huber and G. Herzberg, *Molecular spectra and molecular structure. IV. Constants of diatomic molecules*, Van Nostrand Reinhold Ltd, New York, 1979.
76 H. Ding, M. D. Morse and J. P. Maier, Vibronic analysis of the band system of BNB, *Mol. Phys.*, 2007, **105**, 1251–1261.
77 J. Wang, L. Zhang, G. Zhao, Y. Gu, Z. Zhang, F. Zhang and W. Wang, Selective synthesis of boron nitride nanotubes by self-propagation high-temperature synthesis and annealing process, *J. Solid State Chem.*, 2011, **184**, 2478–2484.
78 V. Jourdain and C. Bichara, Current understanding of the growth of carbon nanotubes in catalytic chemical vapour deposition, *Carbon*, 2013, **58**, 2–39.
79 V. A. Schweigert and I. V. Schweigert, Coagulation in a low-temperature plasma, *J. Phys. D: Appl. Phys.*, 1996, **29**, 655.
80 U. Kortshagen and U. Bhandarkar, Modeling of particulate coagulation in low pressure plasmas, *Phys. Rev. E: Stat. Phys., Plasmas, Fluids, Relat. Interdiscip. Top.*, 1999, **60**, 887–898.
81 P. Kappler, P. Ehrburger, J. Lahaye and J.-B. Donnet, Fine carbon particle formation by carbon-vapor condensation, *J. Appl. Phys.*, 1979, **50**, 308–318.
82 S. Yatom, J. Bak, A. Khrabryi and Y. Raitses, Detection of nanoparticles in carbon arc discharge with laser-induced incandescence, *Carbon*, 2017, **117**, 154–162.
83 L. D. Landau and E. M. Lifshitz, *Statistical Physics*, Translated from the Russian by J. B. Sykes and M. J. Kearsley, Pergamon, 3rd edn, 1969, part 1, vol. 5.
84 B. Glorieux, M. L. Saboungi and J. E. Enderby, Electronic conduction in liquid boron, *Europhys. Lett.*, 2001, **56**, 81–85.
85 M. S. Benilov and G. V. Naidis, Ionization layer at the edge of a fully ionized plasma, *Phys. Rev. E: Stat. Phys., Plasmas, Fluids, Relat. Interdiscip. Top.*, 1998, **57**, 2230–2241.
86 S. E. Nielsen and T. A. Bak, Hard-Sphere Model for the Dissociation of Diatomic Molecules, *J. Chem. Phys.*, 1964, **41**, 665, DOI: 10.1063/1.1725944.

87 Y. B. Zeldovich and Y. P. Raizer, in *Physics of shock waves and high-temperature hydrodynamic phenomena*, ed. W. D. Hayes and R. F. Probstein, Acdemic Press, New York and London, 1966, vol. 1.

88 K. Thielen and P. Roth, N atom measurements in high-temperature $N_2$ dissociation kinetics, *AIAA J.*, 1986, **24**, 1102–1105, DOI: 10.2514/3.9398.

89 L. I. Avramenko and V. M. Krasnenkov, Reactions of nitrogen atoms communication. 4. Rate constant and mechanism of the elementary reaction of nitrogen atoms with molecular hydrogen, *Bull. Acad. Sci. USSR, Div. Chem. Sci.*, 1966, **15**, 394–397.

90 A. M. Mebel, L. V. Moskaleva and M. C. Lin, *Ab initio* MO calculations for the reactions of $NH_2$ with $H_2$, $H_2O$, $NH_3$ and $CH_4$: prediction of absolute rate constants and kinetic isotope effects, *THEOCHEM*, 1999, **461**, 223–238.

91 J. Deppe, G. Friedrichs, A. Ibrahim, H.-J. Romming and H. G. Wagner, The thermal decomposition of $NH_2$ and NH radicals, *Ber. Bunsenges. Phys. Chem.*, 1998, **102**, 1474–1485.



 